Available online at www.sciencedirect.com

ScienceDirect

European Journal of Protistology 69 (2019) 117–137

European Journal of PROTISTOLOGY

www.elsevier.com/locate/ejop

A huge diversity of metopids (Ciliophora, Armophorea) in soil from the Murray River floodplain, Australia. III. Morphology, ontogenesis and conjugation of *Metopus boletus* nov. spec., with implications for the phylogeny of the SAL supercluster

Peter Vďačný[a,*], Wilhelm Foissner[b]

[a] *Department of Zoology, Faculty of Natural Sciences, Comenius University in Bratislava, Ilkovičova 6, Mlynská dolina B-1, 842 15 Bratislava, Slovak Republic*

[b] *FB Ecology and Evolution, Faculty of Natural Sciences, Paris Lodron University of Salzburg, Hellbrunnerstrasse 34, 5020 Salzburg, Austria*

Received 15 February 2019; received in revised form 15 March 2019; accepted 4 April 2019
Available online 13 April 2019

Abstract

The morphology, ontogenesis, conjugation, and phylogenetic position of *Metopus boletus* nov. spec. were studied using live observation, various silver impregnation methods, scanning electron microscopy, morphometry, and the 18S rRNA gene sequence. The new species is outstanding in having a mushroom-like appearance; a globular to broadly ellipsoid macronucleus in anterior body half; 5–10 elongated caudal cilia; 4–6 dikinetids curved rightwards in the anterior portion of the first postoral kinety; and an adoral zone composed of an average of 28 small polykinetids. Ontogenesis of *M. boletus* follows the metopid mode and the species-specific vegetative morphology is obtained after division. Its conjugation is temporary, isogamic and the partners unite ventral-to-dorsal, forming strongly arched to almost rod-like pairs, which indicates a heteropolar arrangement. There are only two maturation divisions and a single synkaryon division in exconjugants. The conjugation data corroborate a sister group relationship of the classes Armophorea and Litostomatea within the SAL (Spirotrichea + Armophorea + Litostomatea) supercluster in that the partners unite ventral-to-dorsal and the main body axes are antiparallel. On the other hand, the last common ancestor of the spirotricheans very likely had a ventral-to-ventral and homopolar conjugation mode with the main body axes oriented in parallel.

Keywords: Conjugation mode; Litostomatea; Maturation divisions; Metopida; Spirotrichea; Stomatogenesis

Introduction

Taxonomy and phylogeny of the order Metopida Jankowski, 1980 got much attention in the last years (e.g., Bourland and Wendell 2014; Bourland et al. 2014, 2017, 2018; da Silva-Neto et al. 2016; Foissner 2016a, 2016b; Omar et al. 2017; Vďačný and Foissner 2017a, 2017b; Vďačný et al. 2019). This globally distributed group of anaerobic, bacterivorous ciliates (e.g., Foissner 2016a, 2016b; Foissner et al. 1992; Tirjaková et al. 2016) has been proven to be as diverse as previously anticipated (Jankowski 1964; Kahl 1926, 1927, 1929, 1932) but our view on phylogeny and systematic position of these elegant creatures has changed considerably (Vďačný et al. 2019). For a long time, the Metopida were considered as a subgroup of heterotrichs, which were traditionally assigned to the Spirotrichea Bütschli, 1889 due to the prominent adoral zone of membranelles/polykinetids

*Corresponding author.
E-mail address: vdacny@fns.uniba.sk (P. Vďačný).

https://doi.org/10.1016/j.ejop.2019.04.002
0932-4739/

(Corliss 1979; Jankowski 1964; Lynn and Small 2002). It was a great surprise when early molecular phylogenetic studies excluded the Metopida from the heterotrichs and suggested a relationship with the class Litostomatea Small and Lynn, 1981 (Embley and Finlay 1994; Hammerschmidt et al. 1996; Hirt et al. 1995) which is, in contrast, characterized by a comparatively simple oral ciliature (Foissner and Agatha 1999). The relatedness of Metopida and Litostomatea was not rejected when further species from all main ciliate lineages were added in 18S rRNA gene phylogenies but the statistical support usually remained poor (for review, see Vďačný et al. 2010).

Lynn (2004) assigned the Metopida to a separate class, Armophorea, which clustered together with the Spirotrichea and the Litostomatea in the extensive phylogenomic analyses based on 158 genes (Gentekaki et al. 2014, 2017). This superclade received high statistical support and was designated as SAL (Spirotrichea + Armophorea + Litostomatea) supercluster. However, interrelationships within the SAL supercluster have been left unresolved although over hundred genes were used to infer their phylogeny (Chen et al. 2018; Gentekaki et al. 2014, 2017; Lynn and Kolisko 2017; Lynn et al. 2018). Interestingly, we have assembled a body of morphological and ultrastructural data that can help to clarify the intricate sister-group relationships within the SAL supercluster. First, Foissner and Agatha (1999) found some common ontogenetical features between the Metopida and the Litostomatea, which were fully corroborated by our recent ontogenetic data from *Lepidometopus platycephalus* Foissner and Vďačný in Vďačný and Foissner, 2017b, a new metopid from floodplain soil of the Murray River in Southeast Australia. Furthermore, Vďačný et al. (2010) recognized that the Armophorea and the Litostomatea share an important ultrastructural synapomorphy, viz., plate-like arranged postciliary microtubule ribbons forming a layer right of and between the ciliary rows.

In this study, for the first time, we describe in detail body, nuclear and ciliary changes during and after conjugation of a metopid. Our comparative analyses reveal that the metopid conjugation mode provides a rich source of evidence that the Armophorea are much more similar to the Litostomatea than to the Spirotrichea. Thus, not only ontogenesis and cortex ultrastructure but also conjugation corroborates the Lamellicorticata hypothesis of a sister group relationship of armophoreans and litostomateans (Vďačný et al. 2010).

Material and Methods

Metopus boletus nov. spec. was discovered in the upper 5 cm soil layer of the floodplain of the Murray River at the Landside of Ryans road near to the town of Albury, Southeast Australia (S36°06′ E146°54′). A detailed description of sampling and sample processing was provided in our previous studies (Vďačný and Foissner 2017a, 2017b). Briefly, *M. boletus* was studied using a combination of in vivo observation, various silver impregnation techniques, scanning electron microscopy (SEM) and morphometry, as described by Foissner (2014). Live ciliates were examined with an optical microscope equipped with bright field and differential interference contrast. The ciliature was revealed with protargol and silver carbonate impregnation. The ontogenetic and conjugation processes were reconstructed from protargol preparations, which show concomitantly body shape, ciliary pattern, and nuclear apparatus. In vivo measurements were realized at 40–1000× while counts and measurements of protargol-impregnated specimens were performed at a magnification of 1000× . Illustrations of live specimens were based on free-hand sketches and photographs while those of impregnated cells were made with a drawing device.

General terminology follows Lynn (2008). Interphase terminology is based on Kahl (1932); Foissner and Agatha (1999) and Vďačný and Foissner (2017a). Conjugation terminology follows Raikov (1972); Xu and Foissner (2004) and Vďačný and Foissner (2008).

ZooBank registration number of the present work (Recommendation 8 A of the International Commission on Zoological Nomenclature 2012) is urn:lsid:zoobank.org:pub:3C8E5A6E-1DF2-403E-9A5A-C5DB2B29F6BB. Since this is mainly a taxonomic study, nomenclatural references are also listed in the ‘Reference’ section.

Results

Metopus boletus Foissner and Vďačný nov. spec

2019 *Metopus* sp. – Vďačný, Rajter, Stoeck and Foissner, J. Eukaryot. Microbiol., 66: 170 (18S rRNA gene sequence, accession no. MH086825).

ZooBank registration number: urn:lsid:zoobank.org:act:2AB298F5-A8BE-48FC-B6E7-3C76A026D4E7.

Diagnosis: Size about 65 × 40 μm in vivo. Preoral dome distinctly overhangs broadly to narrowly obovate postoral body portion, providing a mushroom-like appearance in ventral view. Macronucleus between anterior and posterior end of adoral zone, globular to broadly ellipsoid; one globular to broadly ellipsoid micronucleus. Contractile vacuole and cytopyge terminal. On average 18 ciliary rows on ventral and dorsal side, preoral dome nude; anterior portion of first postoral kinety curved rightwards and composed of 4–6 narrowly spaced dikinetids; 5–10 elongated caudal cilia up to 20 μm long. Perizonal stripe composed of five kineties extending approximately 43% of body length and forming about 46 false kineties. Adoral zone extends about 42% of body length, composed of an average of 28 small polykinetids.

Type locality: Loamy soil and leaf litter from the floodplain of the Murray River near to the town of Albury, Australia (S36°06′ E146°54′).

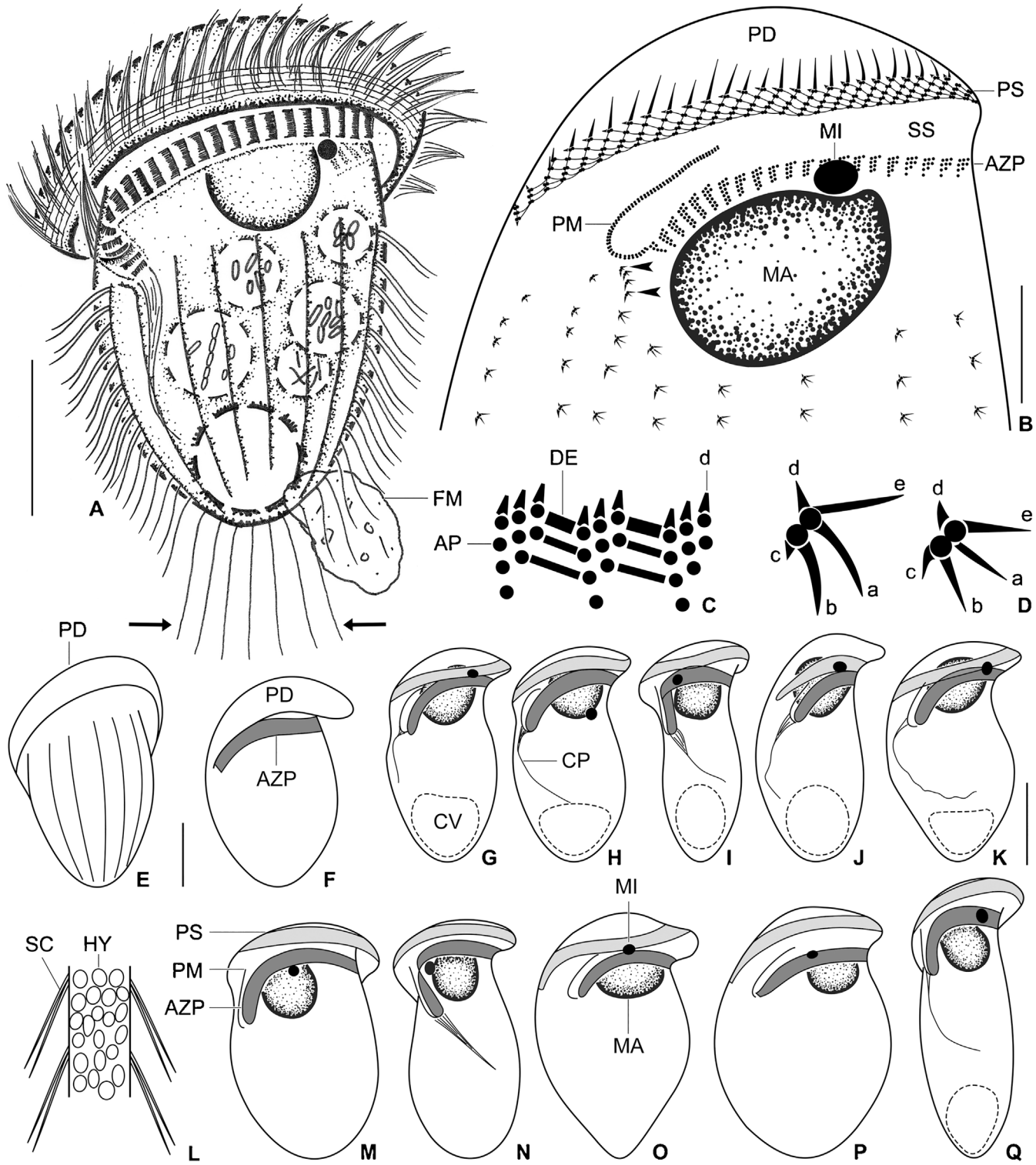

Fig. 1. (**A–Q**) *Metopus boletus* nov. spec. from life (A, E, F, L), and after silver carbonate (B–D) and protargol (G–K, M–Q) impregnation. (**A**) Ventral view of a representative specimen, length 65 μm. Opposed arrows denote the elongated caudal cilia. (**B**) Infraciliature of anterior body half and nuclear apparatus. Arrowheads mark the curved anterior end of the first postoral kinety. (**C**) Fine structure of adoral polykinetids. (**D**) Fibrillar associates of somatic dikinetids. (**E–K, M–Q**) Variability of body shape and size as well as of nuclear apparatus in ventral and ventrolateral views. (**L**) Surface view showing hydrogenosomes arranged in four or five rows between adjacent kineties. a–e, fibrillar associates; AP, adoral polykinetid; AZP, adoral zone of polykinetids; CP, cytopharynx; CV, contractile vacuole; DE, desmoses; FM, faecal mass; HY, hydrogenosomes; MA, macronucleus; MI, micronucleus; PD, preoral dome; PM, paroral membrane; PS, perizonal stripe; SC, somatic cilia; SS, side stripe. Scale bars: 10 μm (B) and 20 μm (A, E–K, M–Q).

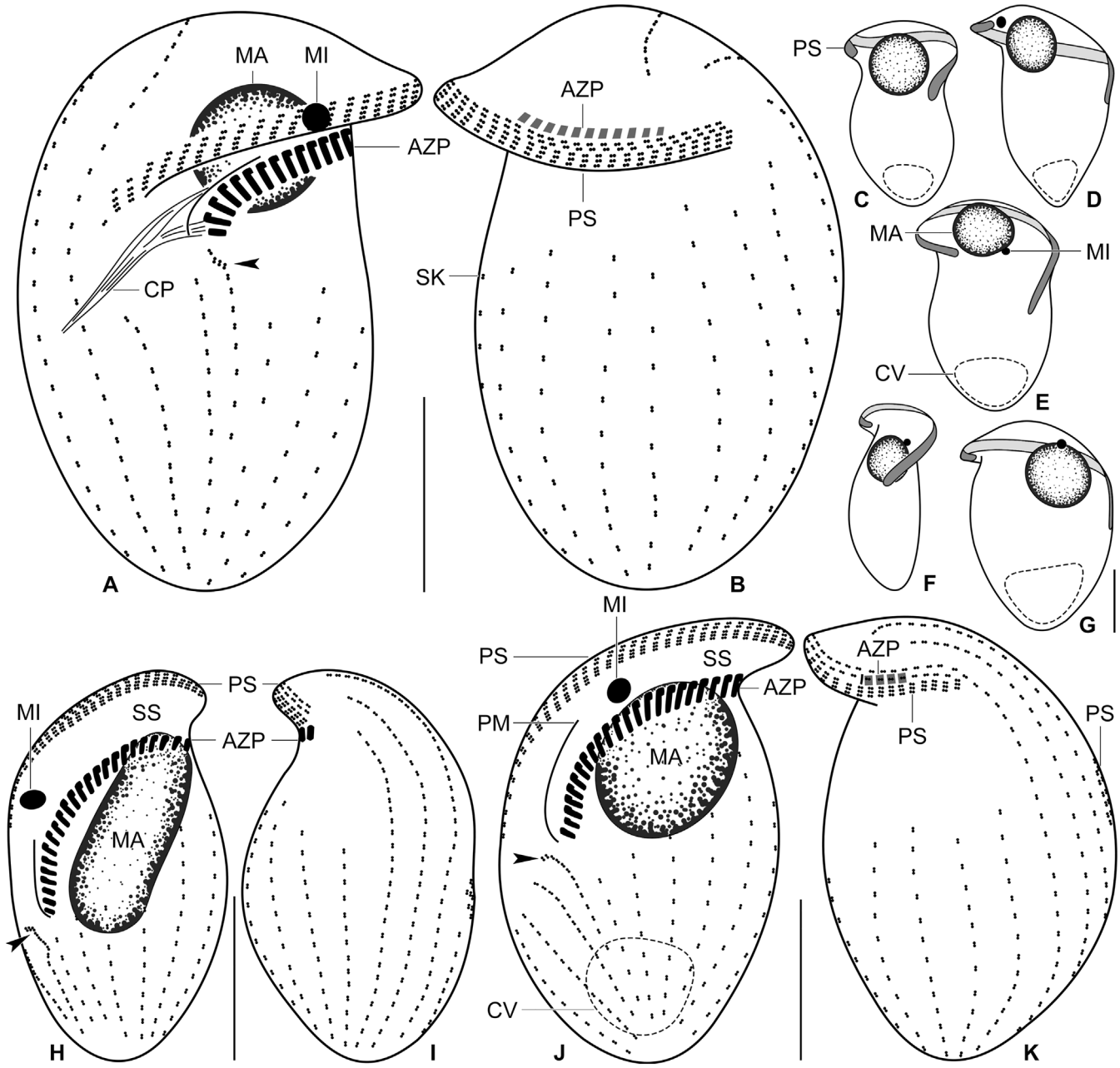

Fig. 2. (**A–K**) *Metopus boletus* nov. spec. after protargol impregnation. (**A, B**) Ventrolateral and dorsolateral ciliary pattern as well as nuclear apparatus of holotype specimen, length 58 μm. (**C–G**) Variability of body shape and size as well as of nuclear apparatus in dorsal and dorsolateral views. Dorsal portion of perizonal stripe is shaded darker than ventral portion. Drawn to scale. (**H–K**) Ventral (H, J) and dorsal (I, K) views of ciliary pattern and nuclear apparatus in an early (H, I) and in a late (J, K) post-divider. Arrowheads mark the narrowly spaced dikinetids of the first postoral kinety. AZP, adoral zone of polykinetids; CP, cytopharynx; CV, contractile vacuole; MA, macronucleus; MI, micronucleus; PM, paroral membrane; PS, perizonal stripe; SK, somatic kinety; SS, side stripe. Scale bars: 20 μm.

Type material: The holotype slide and eight paratype slides with protargol-impregnated specimens have been deposited in the Museum of Natural History (Biologiezentrum) in Linz (LI), Austria. The holotype (Fig. 2A,B) and relevant paratype specimens as well as dividers and conjugants have been marked by black ink circles on the coverslip.

Gene sequence: The 18S rRNA gene sequence of *Metopus boletus* has been deposited in GenBank (accession no. MH086825) under the name "*Metopus* sp. VRSF" by Vďačný et al. (2019). The sequence is 1712 nucleotides long and has a GC content of 44.16%.

Etymology: The Latin noun *boletus* (mushroom) refers to the mushroom-like appearance of this species. The species-group name is treated as a noun in the nominative singular standing in apposition to the generic name (Art. 11.9.1.2 of the International Commission on Zoological

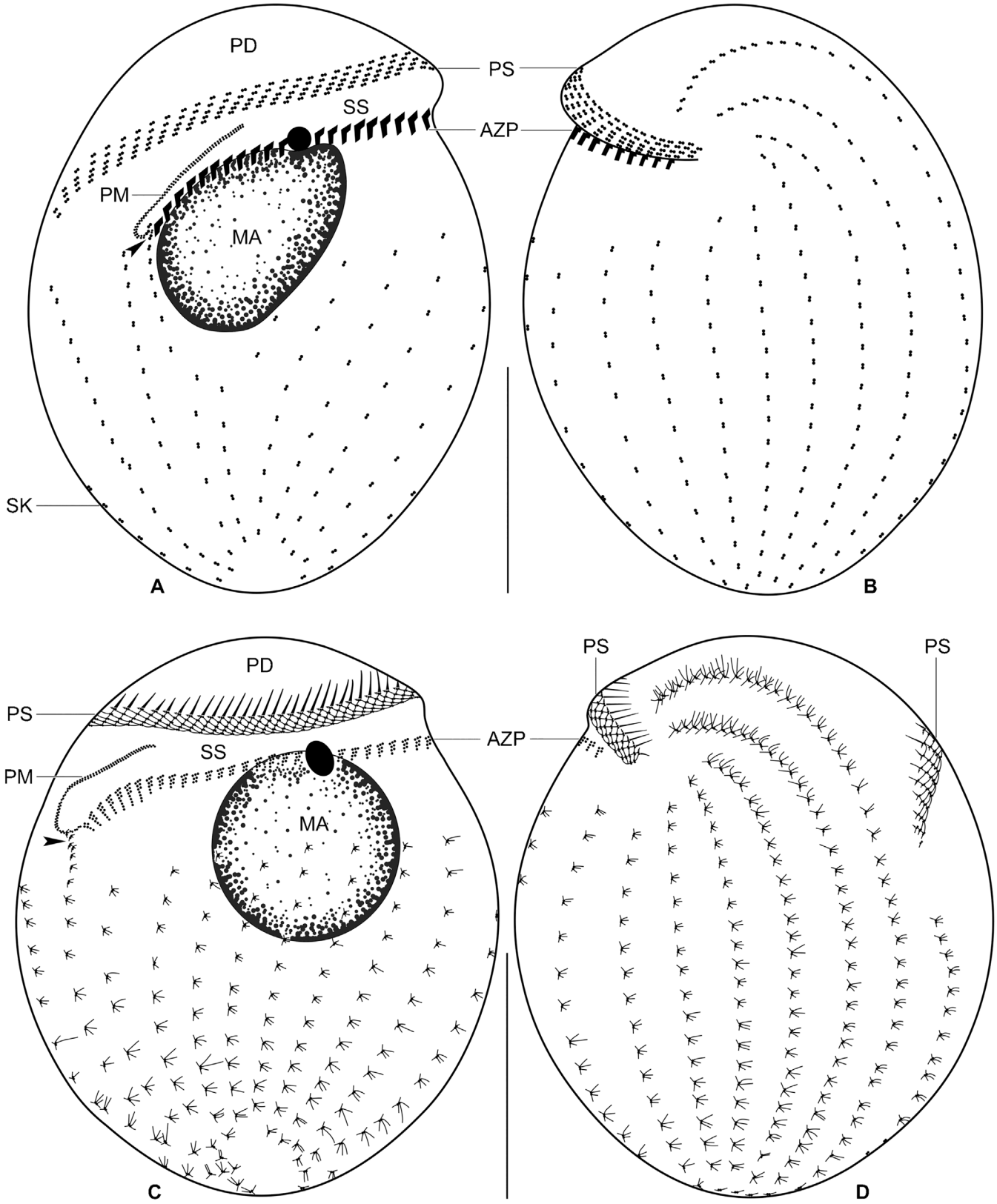

Fig. 3. (**A–D**) *Metopus boletus* nov. spec., infraciliature of ventral (A, C) and dorsal (B, D) side after silver carbonate impregnation. Arrowheads mark the narrowly spaced dikinetids of the first postoral kinety. AZP, adoral zone of polykinetids; MA, macronucleus; PD, preoral dome; PM, paroral membrane; PS, perizonal stripe; SK, somatic kinety; SS, side stripe. Scale bars: 20 μm.

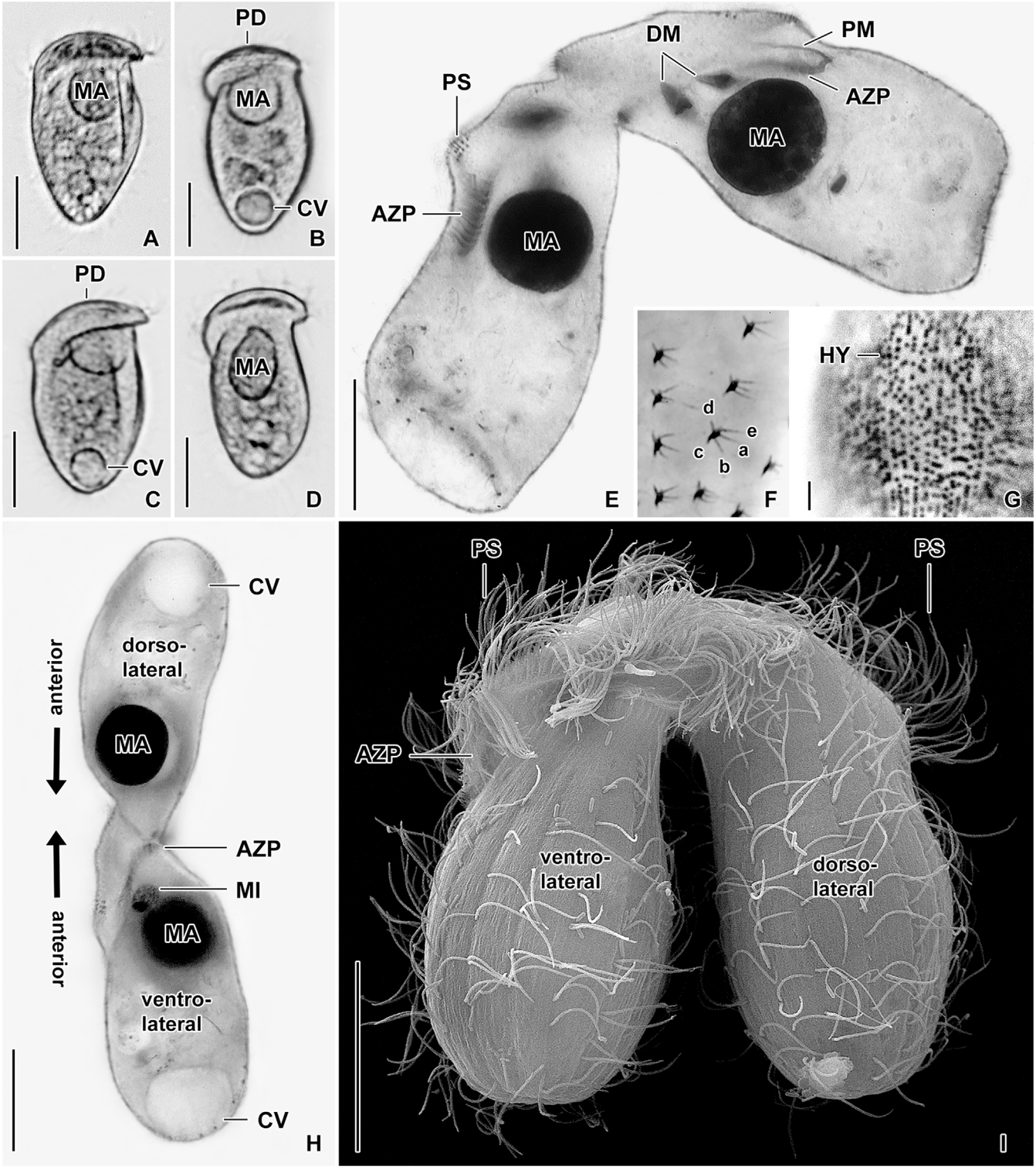

Fig. 4. (**A–I**) *Metopus boletus* nov. spec. from life (A–D), after silver carbonate (F) and protargol (E, G, H) impregnation, and in the scanning electron microscope (I). (**A–D**) Variability of freely motile specimens in body shape and size as well as in nuclear apparatus. (**E, I**) Strongly arched conjugation pairs, showing that the lateral margins of the preoral dome serve as fusion area. (**F**) Fibrillar associates of somatic dikinetids (cp. with Fig. 1D). (**G**) Surface view showing hydrogenosomes. (**H**) Rod-like conjugation pair, showing that the main body axes are clearly antiparallel, which is suggestive of a heteropolar conjugation mode. a–e, fibrillar associates; AZP, adoral zone of polykinetids; CV, contractile vacuole; DM, dividing maturation derivatives; HY, hydrogenosomes; MA, macronucleus; MI, micronucleus; PD, preoral dome; PM, paroral membrane; PS, perizonal stripe. Scale bars: 1 μm (G) and 20 μm (a–e, H, I).

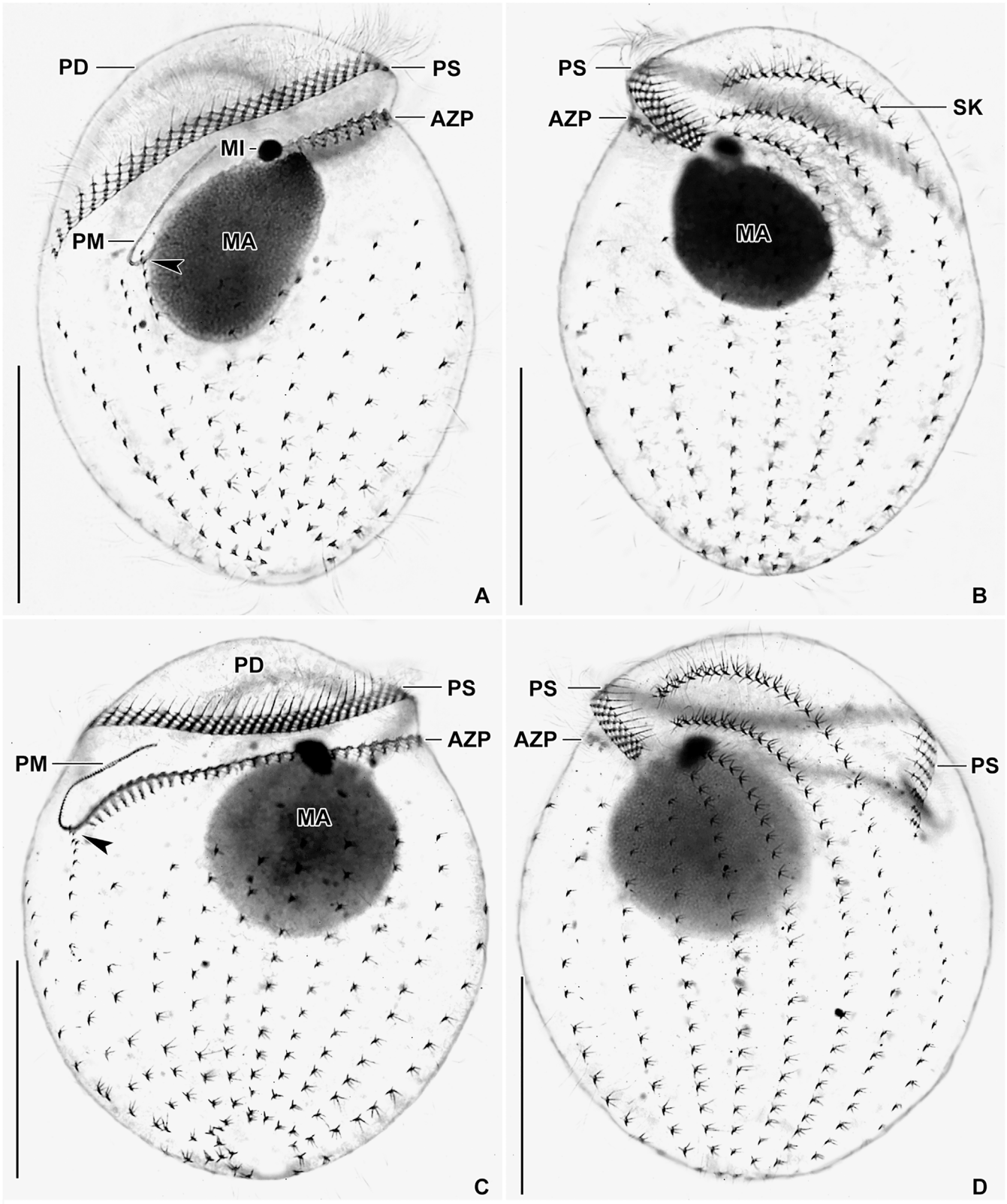

Fig. 5. (**A–D**) *Metopus boletus* nov. spec., infraciliature of ventral (A, C) and dorsal (B, D) side as well as nuclear apparatus after silver carbonate impregnation. Arrowheads mark the narrowly spaced dikinetids of the first postoral kinety, a characteristic feature of the new species. For details of the fibrillar system, see Figs 1B–D and 4 F. AZP, adoral zone of polykinetids; MA, macronucleus; MI, micronucleus; PD, preoral dome; PM, paroral membrane; PS, perizonal stripe; SK, somatic kinety. Scale bars: 20 μm.

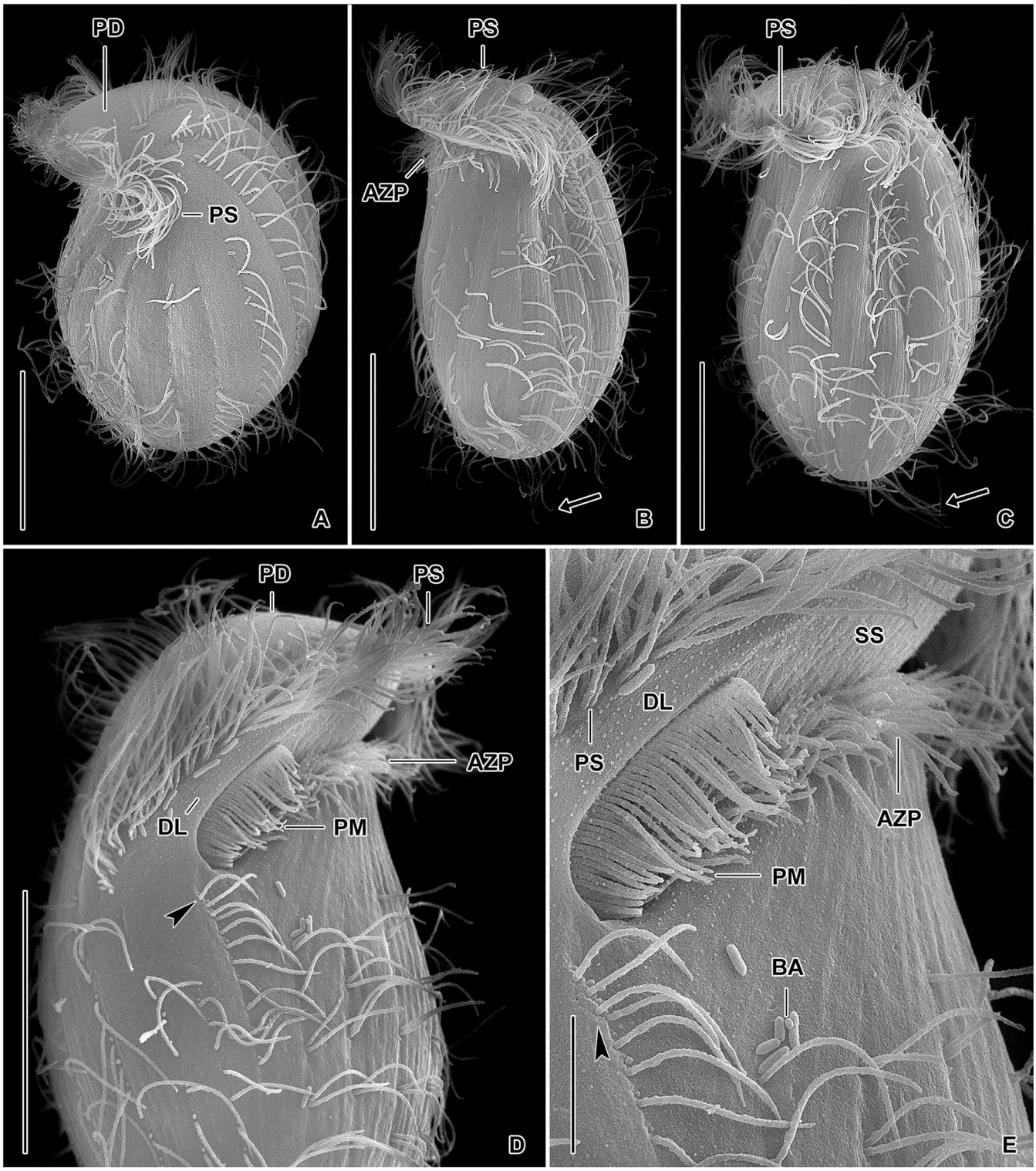

Fig. 6. (**A–E**) *Metopus boletus* nov. spec. in the scanning electron microscope. (**A–C**) Dorsolateral overviews, showing the anteriorly twisted body, the distinctly flattened preoral dome carrying a conspicuous perizonal stripe, and the cortex furrowed by ciliary rows. Arrows denote the elongated caudal cilia. (**D, E**) Ventrolateral overviews of anterior body half and details of oral apparatus. The paroral membrane extends along the margin of the preoral dome and sinks, together with the adoral zone of polykinetids, into the shallow buccal cavity. Note that both basal bodies of some somatic dikinetids are ciliated, an unusual feature in metopids where typically only the posterior basal body is ciliated. Arrowheads mark the curved anterior end of the first postoral kinety. AZP, adoral zone of polykinetids; BA, bacteria; DL, dome lip; PD, preoral dome; PM, paroral membrane; PS, perizonal stripe; SS, side stripe. Scale bars: 5 μm (E) and 20 μm (A–D).

Table 1. Morphometric data on *Metopus boletus* nov. spec.

Characteristic[a]	Mean	M	SD	SE	CV	Min	Max	n
Body, length	57.6	56.0	6.0	1.3	10.4	45.0	68.0	21
Body, maximum width of preoral dome	34.4	32.0	6.5	1.4	19.0	24.0	47.0	21
Body, width at cytostome	28.0	25.0	8.7	1.9	31.2	17.0	43.0	21
Body, maximum postoral width	31.3	31.0	8.4	1.8	26.7	19.0	43.0	21
Body, length:width ratio	1.9	1.8	0.5	0.1	24.5	1.4	3.0	21
Anterior body end to proximal end of PS, distance	25.1	23.0	6.3	1.4	25.3	18.0	38.0	21
Perizonal stripe, percentage of body length	43.3	42.9	8.1	1.8	18.7	29.5	56.9	21
Anterior body end to distal end of AZP, distance	6.4	6.0	2.1	0.5	32.1	4.0	11.0	21
Anterior body end to proximal end of AZP, distance	24.2	24.0	4.7	1.0	19.5	18.0	33.0	21
Adoral zone of polykinetids, percentage of body length	41.9	41.5	5.3	1.2	12.7	34.4	50.8	21
Anterior body end to distal end of PM, distance	10.7	10.0	3.5	0.8	33.0	6.0	20.0	21
Anterior body end to macronucleus, distance	6.8	7.0	2.1	0.5	31.4	2.0	10.0	21
Macronucleus, length	15.6	15.0	2.8	0.6	17.8	12.0	22.0	21
Macronucleus, width	13.5	12.0	2.5	0.5	18.4	11.0	18.0	21
Macronucleus, length:width ratio	1.2	1.2	–	–	–	1.0	1.5	21
Macronucleus, number	1.0	1.0	0.0	0.0	0.0	1.0	1.0	21
Micronucleus, length	2.8	3.0	–	–	–	2.0	3.0	21
Micronucleus, width	2.4	2.0	–	–	–	2.0	3.0	21
Micronucleus, length:width ratio	1.2	1.2	–	–	–	1.0	1.5	21
Micronucleus, number	1.0	1.0	0.0	0.0	0.0	1.0	1.0	21
Somatic ciliary rows, total number	18.3	18.0	1.6	0.3	8.7	15.0	21.0	21
Perizonal ciliary rows, number	5.0	5.0	0.0	0.0	0.0	5.0	5.0	21
False kineties in perizonal stripe, number	45.8	44.0	6.1	1.3	13.3	38.0	59.0	21
Adoral polykinetids, number	28.4	28.0	2.9	0.6	10.4	24.0	34.0	21
Paroral membrane, length	13.7	13.0	2.8	0.6	20.6	10.0	19.0	21

[a]Data based on mounted, protargol-impregnated, and randomly selected specimens from a non-flooded Petri dish culture. Measurements in μm. AZP — adoral zone of polykinetids; CV — coefficient of variation (%); M — median; Max — maximum; Mean — arithmetic mean; Min — minimum; n — number of individuals investigated; PM — paroral membrane; PS — perizonal stripe; SD — standard deviation; SE — standard error of arithmetic mean.

Nomenclature 1999).

Description: Size in vivo 50–80 × 30–55 μm, usually about 65 × 40 μm, as calculated from some in vivo measurements and morphometric data adding 15% preparation shrinkage (Foissner et al. 2002, p. 34). Body twisted anteriorly; length:width ratio ranging from 1.4:1 to 3.0:1 after protargol impregnation and in SEM preparations. Preoral dome moderately convex, with thin distal margin, distinctly overhangs broadly to narrowly obovate postoral body portion and thus producing a mushroom-like appearance in ventral view, usually appears dark at low magnification (40×) because studded with 0.5–2.0 μm-sized lipid droplets; rear body end narrowly to broadly rounded (Figs. 1A, E–K, M–Q, 2 A–G, 4 A–D, 6 A–D; Table 1). Nuclear apparatus typically between anterior and posterior end of adoral zone both in vivo and after protargol impregnation, usually displaced below adoral zone after silver carbonate impregnation. Macronucleus globular to broadly ellipsoid, with a length:width ratio of 1.0–1.5:1, 12–22 × 11–18 μm in size in protargol preparations; nucleoli 1–3 μm across, globular, and evenly distributed. Micronucleus attached to macronucleus at various positions but usually at or near anterior pole of macronucleus; globular to broadly ellipsoid, 2–3 μm in protargol preparations (Figs. 1A, B, G–K, M–Q, 2 A, C–G, 3 A, C, 4 A, B, D, 5 A–D; Table 1). A large contractile vacuole in posterior body end (Figs. 1A, G–K, Q, 2 C–E, G, 4 B, C). Faecal mass slimy, moves through contractile vacuole when expelled via cytopyge (Fig. 1A). Cortex flexible, slightly furrowed by ciliary rows both in vivo and in SEM, sometimes with scattered epibiotic bacteria 1.0–2.5 μm long (Figs. 1E, 6 A–E); no cortical granules recognizable. Conspicuous, mitochondria-like organelles (most likely hydrogenosomes) beneath cortex, narrowly spaced and forming four or five rows between adjacent kineties, sometimes impregnate deeply with protargol but not with silver carbonate (Figs. 1L, 4 G). Cytoplasm colourless, contains some food vacuoles about 12–15 μm across and defecation vacuoles with residues of bacteria; no symbiotic bacteria recognizable in vivo and in protargol preparations. Swims moderately fast, peculiarly wobbling about main body axis due to the curved preoral dome; not very sensitive to oxygen because does not die quickly on microscope slides.

Somatic ciliature composed of dikinetids, often both basal bodies ciliated, sometimes anterior basal body barren or cilia lost during preparation as indicated by no distinct ciliation pattern between dorsal and ventral side; somatic cilia about 12 μm long in vivo; 5–10 caudal cilia up to 20 μm long (Figs. 1A, 6 A–E). On average 18 ciliary rows; all ventral kineties begin posterior to adoral polykinetids, leaving a broad barren stripe posterior to adoral zone, run towards

rear end following body curvature; rarely with breaks or shortened anteriorly or posteriorly; first postoral kinety commences near proximal end of paroral membrane, its anterior end distinctly curved rightwards and composed of 4–6 narrowly spaced dikinetids; left dorsal kineties commence at about same level as ventral kineties and run meridionally, while right dorsal kineties partially extend onto preoral dome and curve towards distal end of perizonal stripe (Figs. 1B, 2 A, B, 3 A–D, 5 A–D, 6 A–E; Table 1). Perizonal stripe begins at left margin of dorsal side, extends slightly obliquely along ventral dome margin and terminates on right margin of dorsal side, length highly variable (CV = 25.3%), i.e., occupies from 29.5% to 56.9%, on average about 43% of body length; invariably composed of five narrowly spaced ciliary rows, segmented into an average of 46 false kineties; each perizonal dikinetid has two cilia 7.0–9.5 μm long in SEM (Figs. 1B, 2 A–G, 3 A–D, 5 A–D, 6 A–D; Table 1).

Somatic dikinetids associated with five fibres after silver carbonate impregnation, possibly corresponding to cathetodesmal fibres (structures "a" and "b"), a postciliary microtubule ribbon (structure "c"), a kinetodesmal fibre (structure "d"), and a transverse microtubule ribbon (structure "e"). Fibres "a" and "b" form a conspicuous V-shaped pattern on left side of dikinetids, extend posteriorly, well recognizable because comparatively long and usually deeply impregnated. Fibre "c" connected to posterior basal body, directed posteriorly to the right, inconspicuous because usually shortest amongst the five basal body associates. Fibre "d" associated with anterior basal body, extends rightwards in an anterior direction, comparatively short, i.e., length only one third to one fourth of fibre "e". Fibre "e" associated with anterior basal body, runs to the left, conspicuous because comparatively long, not impregnated or absent in some dikinetids in anterior and posterior kinety portions (Figs. 1D, 4 F). All fibres very short or not impregnated with silver carbonate in perizonal stripe rows, except for fibres "d" and "e" of perizonal row 5: fibre "d" inconspicuous, short, directed to the right while fibre "e" is very conspicuous because long, thick and deeply impregnated, directed anteriorly and slightly to the left. Dikinetids of perizonal stripe connected by a fine, rectangular mesh of fibres resembling the colpodid silverline pattern, i.e., each dikinetid radiates four fibres in a cross-like pattern: two fibres run anteriorly right- and leftwards and two fibres run posteriorly right- and leftwards. Left anterior and right posterior fibres form main axis of a false kinety while right anterior and left posterior fibres obliquely connect adjacent false kineties (Figs. 1B, 3 C, D, 5 A–D).

Type 1 oral area (for details, see Vďačný and Foissner 2017a, p. 37Vďačný and Foissner, 2017aVďačný and Foissner 2017a, p. 37). Adoral zone distinctly spiralled; length highly variable (CV = 19.5%), i.e., occupies from 34% to 51%, on average 42% of body length; commences posterior to perizonal stripe at left margin of dorsal side and runs slightly obliquely over ventral side to right body margin curving leftwards to sink into shallow buccal cavity; composed of an average of 28 small, L-shaped polykinetids; cilia about 8 μm long in vivo (Figs. 1B, C, 2 A, B, 3 A–D, 5 A–D; Table 1). Individual polykinetids obliquely connected by three desmoses faintly impregnated with silver carbonate: first desmose connects anterior basal body of third short row with anterior basal body of first long row of the adjacent polykinetid, second desmose connects second basal bodies of third short and first long row of the adjacent polykinetid, and third desmose connects posterior basal body of second row with third basal body of first long row of the adjacent kinety. Fibres of basal bodies in polykinetids very short or not impregnated with silver carbonate, except for fibre "d" of anterior basal bodies of each row; fibres "d" inconspicuous, short and directed anteriorly (Fig. 1C). Paroral membrane J-shaped and on average 14 μm long after protargol impregnation; begins about 10 μm posterior from anterior body end and extends along adoral polykinetids to sink into buccal cavity; composed of densely arranged dikinetids, but only one basal body ciliated according to SEM observations, cilia about 10 μm long in vivo (Figs. 1B, 2 A, 3 A, C, 5 A, C, 6 D, E; Table 1). Cytopharyngeal fibres originate from proximal end of adoral zone and paroral membrane, usually curve obliquely leftwards forming a slender funnel about 20 μm long in protargol preparations (Figs. 1A, G–K, N, Q). Dome lip inconspicuous, only 1.9–2.8 μm wide in SEM, dotted by tiny warts arranged in three or four rows as observed in one well oriented specimen (Fig. 6D, E). Side stripe a smooth, moderately deep channel 2.8–5.5 μm wide in SEM (Fig. 6D, E).

Phylogenetic position: According to our previous phylogenetic analyses, *M. boletus* is classified as a sister taxon of *M. laminarius* with full statistical support in Bayesian inferences and maximum likelihood analyses (Vďačný et al. 2019). Both taxa are placed within a highly diverse and variably statistically supported cluster, comprising the free-living *M. minor*, *M. hasei*, *M. yantaiensis* and *Atopospira* spp. as well as the endosymbiotic *Parametopidium circumlabens* and members of the order Clevelandellida (Fig. 7).

Notes on ontogenesis of *Metopus boletus*

Although only few dividers were found in the protargol slides, they document that the ontogenesis of *M. boletus* follows the metopid mode: (1) division takes place in freely motile condition and the body undergoes drastic re-shaping, causing the outline to become ovate in early dividers (Fig. 8C, D), ellipsoid in mid-dividers (Fig. 8E, F) and dumbbell-shaped in late dividers (Fig. 8G, H); (2) stomatogenesis is pleurokinetal and the parental paroral membrane is reorganized but does not contribute to the daughter oral ciliature (Fig. 8C, G, asterisks); (3) the opisthe's adoral polykinetids originate in posterior body half by proliferation of dikinetids in five or six dorsal and dorsolateral as well as some postoral kineties. Very likely, each of these kineties produces two adoral polykinetids (Fig. 8B, C). In mid-dividers, pro-

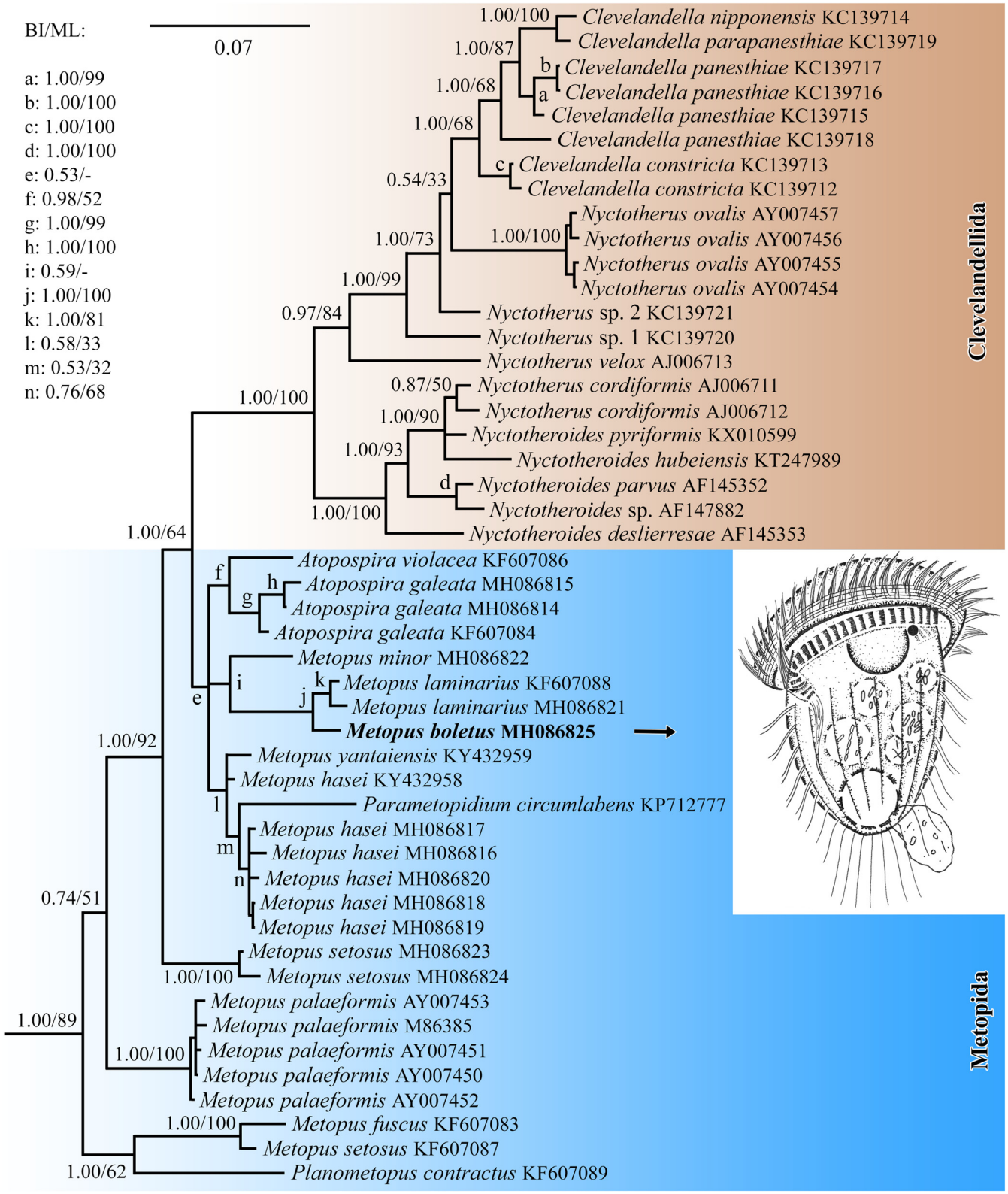

Fig. 7. Nuclear 18S rRNA gene tree of the class Armophorea (from Vďačný et al. 2019), showing the phylogenetic position of *Metopus boletus* nov. spec. Posterior probabilities for Bayesian Inference (BI) and bootstrap values for Maximum Likelihood (ML) are mapped onto the 50%-majority rule Bayesian consensus tree. Dashes indicate mismatch in topology between Bayesian and ML tree. The scale bar denotes seven substitutions per one hundred nucleotide positions. *Planometopus contractus* was originally submitted to GenBank as *Palmarella lata* (Bourland et al. 2014).

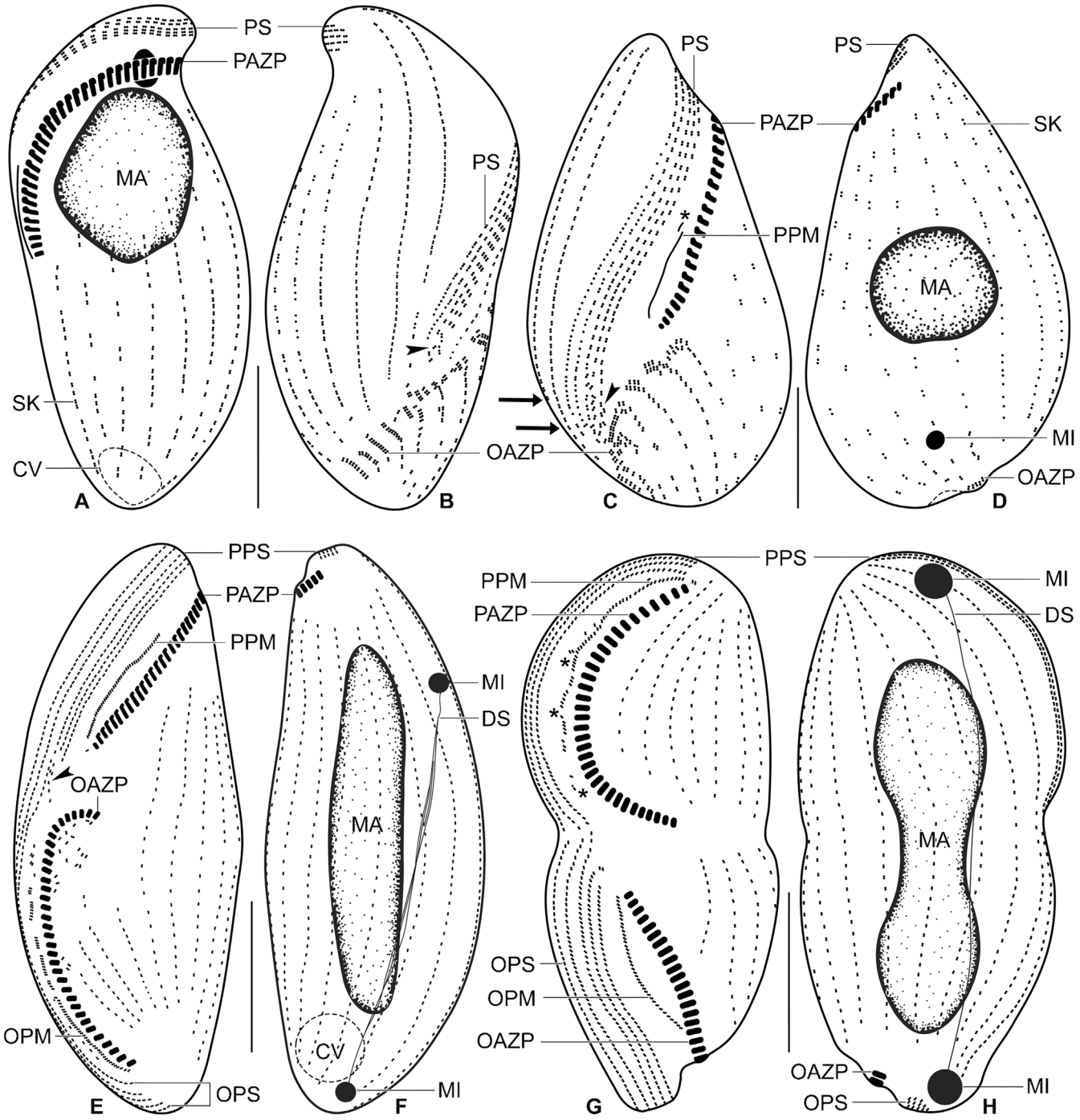

Fig. 8. (**A–H**) *Metopus boletus* nov. spec., ciliary pattern and nuclear apparatus of early dividers (A–D), a mid-divider (E, F), and a late divider (G, H) after protargol impregnation. Division takes place in freely motile condition and the body undergoes drastic re-shaping, becoming ovate in early dividers, fusiform in mid-dividers and dumbbell-shaped in late dividers. Stomatogenesis is pleurokinetal and the opisthe's adoral polykinetids originate in the posterior body half by proliferation of dikinetids in five or six dorsal and dorsolateral as well as some postoral kineties. Arrowheads in (B, C, E) denote scattered dikinetids at posterior end of parental perizonal rows 1 and 2 that migrate along the new adoral membranelles to assemble the opisthe's paroral membrane. Arrows in (C) point to two dorsolateral kineties which migrate towards the growing perizonal stripe to become perizonal rows 4' and 5' in the opisthe. Asterisks in (C, G) mark reorganization of the parental paroral membrane. CV, contractile vacuole; DS, division spindle; MA, macronucleus; MI, micronucleus; OAZP, opisthe's adoral zone of polykinetids; OPM, opisthe's paroral membrane; OPS; opisthe's perizonal stripe; PAZP, proter's adoral zone of polykinetids; PPM, proter's paroral membrane; PPS; proter's perizonal stripe; PS, perizonal stripe; SK, somatic kineties. Scale bars: 20 μm.

topolykinetids detach from the somatic ciliary rows and migrate to assemble the opisthe's adoral zone (Fig. 8E); (4) the opisthe's paroral membrane is produced by the dissociated posterior portion of the first two parental perizonal rows and possibly by some scattered dikinetids from the posterior end of the third parental perizonal row (Fig. 8B, C, E, arrowheads). The new paroral membrane is assembled into a continuous dikinetal row in late dividers (Fig. 8G); (5) the opisthe's perizonal stripe has a hybrid origin, i.e., it is formed by three parental perizonal rows and two dorsolateral ciliary rows: the posterior portions of the parental perizonal rows 3–5 become opisthe's perizonal rows 1'–3' while posterior parts of the first two dorsolateral kineties migrate towards rows 1'–3' to become opisthe's perizonal rows 4' and 5' (Fig. 8C, arrows, G); (6) the macronucleus migrates to mid-body in early dividers (Fig. 8D), assumes a rod-like shape in mid-dividers (Fig. 8F), and becomes dumbbell-shaped in late dividers (Fig. 8H). Micronuclear division commences in mid-dividers (Fig. 8F) and the daughter micronuclei remain connected by a fibre bundle in late dividers (Fig. 8H).

The species-specific vegetative morphology is very likely obtained after division, as usual in metopids (Foissner and Agatha 1999; Vďačný and Foissner 2017b): (1) the body grows and the preoral dome pulls out of the cell and twists leftwards, taking along the adoral zone and the perizonal stripe; (2) the adoral polykinetids become L-shaped and the paroral membrane becomes J-shaped; (3) the anteriormost basal bodies of the first postoral kinety become narrowly spaced and curve rightwards; (4) the first two right dorsal kineties extend onto the preoral dome and curve towards the distal end of the perizonal stripe; (5) the macronucleus shortens to become globular and the micronucleus migrates towards the macronucleus (Fig. 2H–K).

Conjugation of *Metopus boletus*

Conjugation mode

Conjugation is isogamic with respect to body shape and size. The average length ratio of the partners is very stable and ranges from 1.0:1 to 1.1:1, i.e., the length difference between partners is less than 10% (Table 2). One partner places the left margin of the ventral side of the preoral dome onto the right margin of the dorsal side of the dome of the other partner. Thus, the lateral margins of the preoral dome serve as fusion area (Figs. 4I, 10 A, B). The union mode is ventral-to-dorsal with respect to the adoral zone and perizonal stripe. Specifically, when the pair is observed in the same focal plane, the ventral portion of both ciliary structures is visible only in one partner (Fig. 10A, B). Whether conjugation is homo- or heteropolar is difficult to state because the conjugants form strongly arched to almost rod-like pairs (Figs. 4E, H, I, 9 A–G, 10 A, B). Their arrangement is not correlated with progress of conjugation. However, the main body axes are clearly antiparallel in rod-like pairs (Figs. 4H, 9 A, G), which is suggestive of a heteropolar conjugation mode. Conjugation is temporary, i.e., the partners separate after formation of the synkaryon.

Body and ciliary changes

All modifications in body shape and ciliary pattern during and after conjugation are associated with the remodelling of the preoral dome. With the onset of conjugation, the dome flattens and elongates, forming an obtuse angle with the main body axis (Figs. 4E, H, 9A–E, 10 A, B). In comparison with vegetative cells, the body becomes longer (62–82 μm vs. 45–68 μm) and more slender (2.6:1 vs. 1.9:1). Further, the course of the adoral zone and perizonal stripe becomes more oblique and both are much less twisted than in morphostatic specimens. Likewise, the ciliary rows extending onto the preoral dome become almost straight. No changes occur in the postoral ciliature including the densely ciliated, curved anterior portion of the first postoral kinety. Likewise, the adoral zone and the paroral membrane remain unchanged (Fig. 10A, B). Conjugants and vegetative cells have a very similar average number of adoral polykinetids (27 vs. 28), somatic kineties (16 vs. 18), and false kineties (43 vs. 46) as well as a similar length of the paroral membrane (12.3 μm vs. 13.7 μm). This indicates the absence of preconjugation divisions.

Soon after separation, the shape of the exconjugants is very dissimilar from that of vegetative cells due to the remodelled preoral dome. Thus, early exconjugants are the most slender cells in the population because their preoral dome is narrow, only indistinctly twisted, and strongly oblique, forming an obtuse angle with the main body axis. Some irregularities and deformations are still recognizable in the upper portion that served for partner union (Fig. 10C, D). However, body and preoral dome assume the characteristic vegetative morphology comparatively rapidly, i.e., after the first synkaryon division (Fig. 10E, F).

Nuclear changes

There are only two maturation divisions. During the first division, the micronucleus swells from a size of about 3 × 2 μm to 8.2–8.6 × 6.3–6.7 μm (Figs. 4H, 9 A–E; Table 2). In the early prophase, the micronucleus displays an eccentric, deeply impregnated, elliptic plate 3 × 2 μm in size and a bright margin with some argyrophilic granules (Fig. 9A–C). The deeply impregnated plate assumes a narrowly elliptic shape (5 × 2 μm) and becomes localized almost equatorially within the inflated micronucleus during the late prophase (Fig. 9E). The plate is encompassed by a slightly brighter spindle surrounded by the bright nucleoplasm still having some argyrophilic granules. About four filiform chromosomes differentiate from the deeply impregnated central plate. The second division (Figs. 4E, 9 F) yields four maturation derivatives that also impregnate heterogeneously, i.e., they contain a deeply impregnated centre surrounded by brighter nucleoplasm. Two maturation derivatives migrate posteriorly towards the contractile vacuole and begin to decrease in size from about 7 × 4 μm to 3 × 2.5 μm.

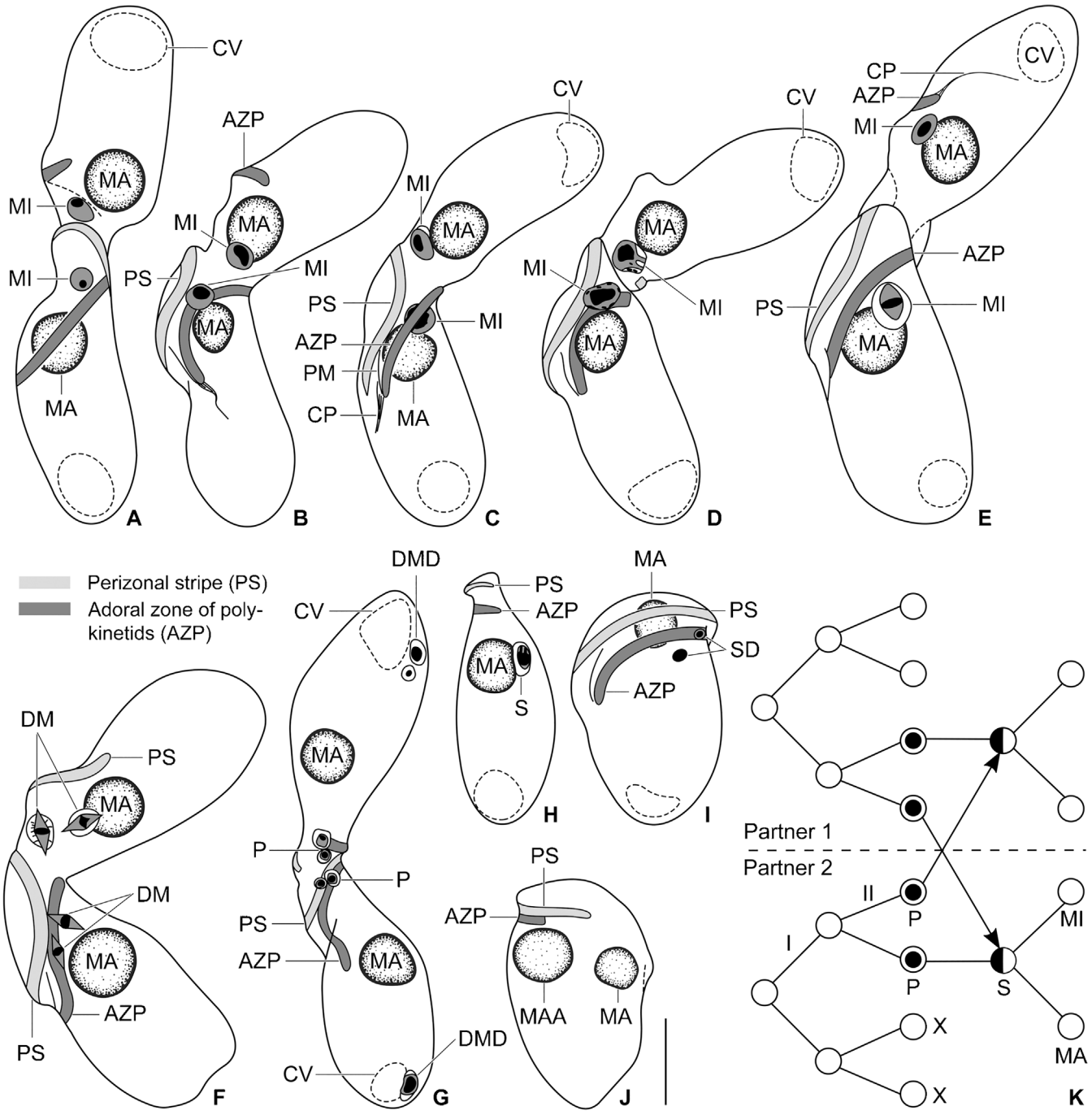

Fig. 9. (**A–K**) *Metopus boletus* nov. spec., body and nuclear changes during and after conjugation in protargol preparations. (**A–E**) Early prophase of the first maturation division. The micronucleus swells from a size of about 3 × 2 μm to 8.5 × 6.5 μm and displays a dark, elliptical structure surrounded by a bright margin. (**F**) Late prophase of the second maturation division. The dark mass assumes a narrowly elliptical shape and becomes localized almost equatorially within the fusiform micronucleus. (**G**) Conjugants after exchange of the pronuclei. (**H**) Early exconjugant with a synkaryon. (**I**) The single synakryon division generates two globular, similarly sized synkaryon derivatives: one differentiates to a new micronucleus while the other enlarges and transforms to a new macronucleus. J: Late exconjugant with the parental macronucleus and a macronucleus anlage. (**K**) Scheme of the nuclear processes during and after conjugation. Two maturation divisions (I, II) and a single synkaryon division produce two synkaryon derivatives: one becomes the micronucleus and other one the macronucleus. Crosses mark degenerating maturation derivatives. AZP, adoral zone of polykinetids; CP, cytopharynx; CV, contractile vacuole; DM, dividing maturation derivatives; DMD, degenerating maturation derivatives; MA, parental macronucleus; MAA, macronucleus anlage; MI, micronucleus; P, pronuclei; PM, paroral membrane; PS, perizonal stripe; S, synkaryon; SD, synkaryon derivatives; X, degenerating maturation derivatives. Scale bar: 20 μm.

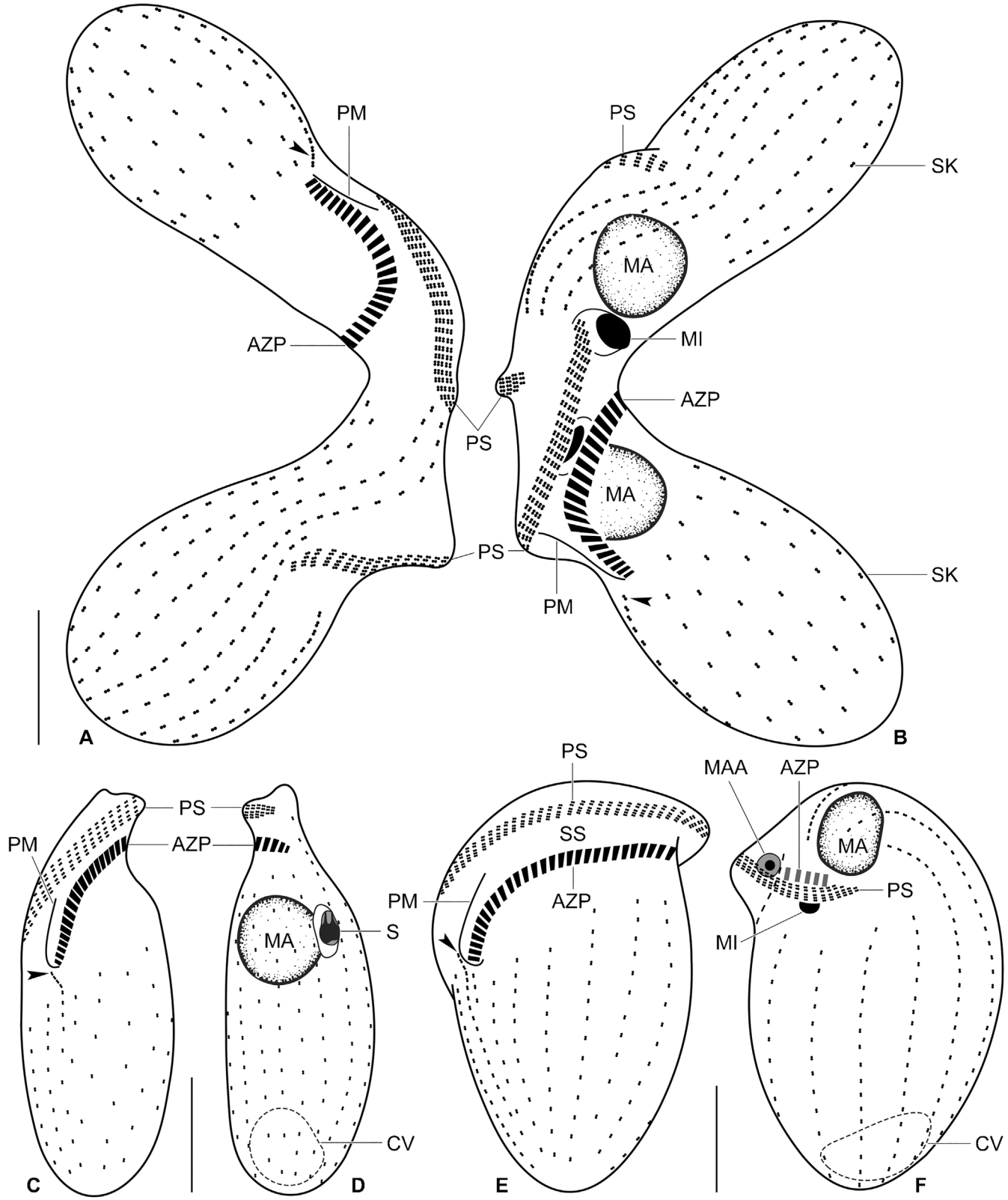

Fig. 10. (**A–F**) *Metopus boletus* nov. spec., ciliary pattern and nuclear apparatus of a conjugation pair (A, B), an early exconjugant (C, D), and a late exconjugant (E, F) after protargol impregnation. Arrowheads mark the curved anterior end of the first postoral kinety. AZP, adoral zone of polykinetids; CV, contractile vacuole; MA, macronucleus; MMA, macronucleus anlage; MI, micronucleus; PM, paroral membrane; PS, perizonal stripe; S, synkaryon; SK, somatic kineties; SS, side stripe. Scale bars: 20 μm.

Table 2. Morphometric data on conjugating *Metopus boletus* nov. spec.

Characteristic[a]	Mean	M	SD	SE	CV	Min	Max	n
Long partner, length	74.8	75.0	5.2	1.6	7.0	66.0	82.0	11
Short partner, length	72.0	70.0	6.0	1.8	8.4	62.0	80.0	11
Partners, length ratio	1.0	1.0	–	–	–	1.0	1.1	11
Long partner, maximum postoral width	28.1	26.0	4.4	1.3	15.8	22.0	36.0	11
Short partner, maximum postoral width	28.3	27.0	3.1	0.9	11.1	25.0	36.0	11
Long partner, length:width ratio	2.7	2.6	0.4	0.1	13.6	2.2	3.6	11
Short partner, length:width ratio	2.6	2.6	–	–	–	2.2	2.8	11
Long partner, perizonal stripe length[b]	40.0	40.0	3.6	1.1	9.1	33.0	47.0	11
Short partner, perizonal stripe length[b]	37.8	39.0	3.5	1.0	9.1	33.0	42.0	11
Long partner, perizonal stripe % of body length	53.5	54.9	4.1	1.2	7.7	48.7	59.5	11
Short partner, perizonal stripe % of body length	52.6	52.5	3.3	1.0	6.3	48.6	58.2	11
Long partner, number of false kineties	42.6	42.0	3.5	1.1	8.2	39.0	50.0	10
Short partner, number of false kineties	43.5	43.5	2.1	0.7	4.8	40.0	46.0	10
Long partner, AZP length	38.2	38.0	3.2	1.0	8.3	34.0	44.0	11
Short partner, AZP length	36.5	36.0	3.9	1.2	10.8	30.0	43.0	11
Long partner, AZP % of body length	51.1	51.4	3.5	1.1	6.9	45.0	55.7	11
Short partner, AZP % of body length	50.7	50.7	3.7	1.1	7.4	44.8	56.7	11
Long partner, number of adoral polykinetids	27.5	28.0	1.6	0.5	5.9	25.0	30.0	11
Short partner, number of adoral polykinetids	27.8	27.0	2.5	0.8	9.1	25.0	33.0	10
Long partner, macronucleus length	15.2	15.0	1.5	0.4	9.7	13.0	18.0	11
Short partner, macronucleus length	16.3	16.0	1.5	0.4	9.2	15.0	20.0	11
Long partner, macronucleus width	13.8	13.0	2.1	0.6	15.5	11.0	17.0	11
Short partner, macronucleus width	14.1	14.0	1.9	0.6	13.3	12.0	19.0	11
Long partner, macronucleus length:width ratio	1.1	1.1	–	–	–	1.0	1.3	11
Short partner, macronucleus length:width ratio	1.2	1.2	–	–	–	1.0	1.3	11
Long partner, micronucleus length[c]	8.2	8.0	1.6	0.5	19.0	5.0	10.0	9
Short partner, micronucleus length[c]	8.6	9.0	1.7	0.6	20.3	6.0	10.0	9
Long partner, micronucleus width[c]	6.7	6.0	1.7	0.6	24.9	4.0	10.0	9
Short partner, micronucleus width[c]	6.3	6.0	1.6	0.5	25.0	5.0	10.0	9
Long partner, micronucleus length:width ratio[c]	1.3	1.3	–	–	–	1.0	1.7	9
Long partner, micronucleus length:width ratio[c]	1.4	1.4	–	–	–	1.0	2.0	9
Long partner, number of somatic kineties	16.3	16.0	1.5	0.5	9.2	14.0	19.0	10
Short partner, number of somatic kineties	16.7	16.5	0.9	0.3	5.7	16.0	19.0	10
Long partner, paroral membrane length	13.0	13.0	1.8	0.6	13.6	10.0	15.0	10
Short partner, paroral membrane length	11.7	12.0	2.0	0.6	16.7	8.0	15.0	11

[a] Data based on mounted, protargol-impregnated, and randomly selected specimens from a non-flooded Petri dish culture. Measurements in μm. AZP — adoral zone of polykinetids; CV — coefficient of variation (%); M — median; Max — maximum; Mean — arithmetic mean; Min — minimum; n — number of individuals investigated; SD — standard deviation; SE — standard error of arithmetic mean.

[b] Measured from anterior to posterior end of perizonal stripe.

[c] In prophase of the first maturation division.

The two remaining maturation derivatives move into the anterior body portion, one becomes a stationary pronucleus while the other transforms into a migratory pronucleus (Fig. 9G). The pronuclei are of unequal size: the migratory pronucleus is about 5 × 3 μm in size while the stationary pronucleus has a size of about 7 × 6 μm. A synkaryon each is formed in the partners by fusion of the migratory pronucleus with the stationary one. The partners separate after the formation of the synkaryon, causing that synkaryon division takes place in the exconjugants. It is characterized by an inflation of the synkaryon which is surrounded by a distinct membrane (Figs. 9H, 10 D). The single synkaryon division generates two globular, similarly sized derivatives (Figs. 9I, 10 F): one differentiates to a new micronucleus, the other enlarges and transforms to a new macronucleus. Exconjugants with two or four macronuclear anlagen were also observed.

The parental macronucleus maintains the globular morphology and is localized in the anterior body half during the maturation divisions (Figs. 4E, H, 9 A–F). Nucleoli are still well recognizable during these initial stages of conjugation. After synkaryon division, the parental macronucleus begins to diminish in size (Fig. 9H). Unlike the degenerating maturation derivatives, the parental macronucleus is still present in late exconjugants along with the intensively growing new macronucleus (Fig. 9I, J).

Discussion

Metopus boletus as a new species

Metopus boletus is distinguished from congeners by a combination of the following characters: (i) a mushroom-like appearance due to the distinctly overhanging preoral dome and the obovate postoral body portion; (ii) a globular to broadly ellipsoid macronucleus in anterior body half; (iii) 5–10 caudal cilia up to 20 μm long; and (iv) the peculiar first postoral kinety whose anterior region is distinctly curved rightwards and composed of 4–6 narrowly spaced dikinetids. The similarly sized and co-occurring *M. murrayensis* Foissner and Vďačný in Vďačný and Foissner, 2017a has also a globular macronucleus and caudal cilia. However, the macronucleus is surrounded by highly refractive granules and the caudal cilia are two times longer, i.e., about 40 μm. *Metopus pulcher* Kahl, 1927 exhibits also an almost globular macronucleus but is easily distinguished from *M. boletus* by the adoral zone which extends about 90% vs. 40% of body length. Interestingly, *Idiometopus turbo* (Dragesco and Dragesco-Kernéis 1986) Bourland et al., 2018 has a stout appearance and a file of narrowly spaced basal bodies postorally. These, however, do not extend towards the paroral membrane but form narrowly spaced, short kineties or remain as disordered dikinetids (Bourland et al. 2018). Moreover, *M. boletus* clearly differs from *I. turbo* also by the shape of the macronucleus which is globular to oval in the former while C-shaped in the latter.

According to 18S rRNA gene phylogenies (Vďačný et al. 2019), *M. boletus* is closely related to the morphologically highly dissimilar *M. laminarius* Kahl, 1927. Both species can be easily distinguished by body shape and size as well as by the macronuclear pattern. *Metopus laminarius* has a slender, 200–260 μm long body and a U-shaped macronucleus in posterior body half. On the other hand, *M. boletus* is much stouter and smaller (50–80 × 30–55 μm) and displays a globular macronucleus in the anterior body half. *Metopus laminarius* f. *minor* Kahl, 1932 very likely represents a distinct species. It is still much larger than *M. boletus* (150 μm vs. up to 80 μm) and its macronucleus is narrowly ellipsoid and in posterior body half (vs. globular to broadly ellipsoid and in anterior body half) (Kahl 1932).

Conjugation

So far, conjugation of metopids has not been investigated in detail, except for the study of Noland (1927) who concentrated on the nuclear events and body changes in *M. sigmoides* [now *M. es* (Müller, 1776) Lauterborn, 1916]. Some anecdotal observations are available on live specimens of *M. mirabilis* Kahl, 1928, *M. es* and *M. violaceus* [now *Atopospira violacea* (Kahl, 1926) Bourland and Wendell, 2014] by Kahl (1932) as well as on *M. fuscus* Kahl, 1927 by Bourland et al. (2014). All basically agree in that pair formation is ventral-to-dorsal. A single exception might be *A. violacea* in which the ventral sides of the partners could overlap laterally according to Fig. 70_{28} in Kahl (1932). But we cannot exclude that this peculiar arrangement might be part of the complex dances leading the partners to come in contact; the final union would be ventral-to-dorsal, as typical for other metopids. Metopid conjugants consistently form an inverted U- or V-shaped pattern, which was interpreted as homopolar in *M. fuscus* by Bourland et al. (2014). The conjugation is anisogamic in *M. fuscus* (Bourland et al. 2014) while it begins isogamic and ends anisogamic in *M. es* whereby the distinctly smaller exconjugant dies after pair separation (Noland 1927). Very likely, this was misinterpreted as total conjugation by Raikov (1972). However, our detailed observations reveal the conjugation of *M. boletus* to be temporary and isogamic (Table 2). Whether the orientation of the partners is homo- or heteropolar is difficult to state. However, the presence of almost rod-like pairs indicates that it is in fact heteropolar but partners can arch, which causes a homopolar-like appearance. Both, strongly arched and rod-shaped pairs occur also in two litostomatean groups, viz., the dileptids (Vďačný and Foissner 2008) and in the spathidiids (Xu and Foissner 2004). However, their conjugation mode is clearly heteropolar since the main body axes of the partners are oriented antiparallelly.

As concerns the nuclear processes, there are only two maturation divisions in *M. boletus* (Fig. 9K) while three in *M. es* (Noland 1927). On the other hand, both *Metopus* species have only one synkaryon division, a number that has been reported also from a rather closely related species, viz., *Nyctotherus cordiformis* (Golikowa 1965; Wichterman 1937) from the endosymbiotic order Clevelandellida de Puytorac and Grain, 1976. Although nuclear phenomena seem to be species specific, only two maturation divisions and one synkaryon division have been reported in several species of the endosymbiotic order Entodiniomorphida Reichenow in Doflein and Reichenow, 1929 (e.g., *Diplodinium ecaudatum*, *D. triloricatum*, *Entodinium caudatum*, *Cycloposthium bipalmatum*; for details, see Raikov 1972) from the class Litostomatea which is rather closely related to the class Armophorea (e.g., Chen et al. 2018; Gentekaki et al. 2014; Vďačný et al. 2010). Nevertheless, the phylogenetic position of entodiniomorphids indicate that this pattern evolved convergently, since the last common ancestor of the class Litostomatea very likely had three maturation divisions and usually two or three synkaryon divisions. Indeed, this pattern is distributed in a broad variety of litostomateans, e.g., in the endosymbiotic *Balantidium* as well as in free-living dileptids, spathidiids and didiniids (Raikov 1972; Vďačný and Foissner 2008; Xu and Foissner 2004 and references cited therein).

Phylogeny

Extensive transcriptome analyses united the classes Spirotrichea, Armophorea and Litostomatea, forming the

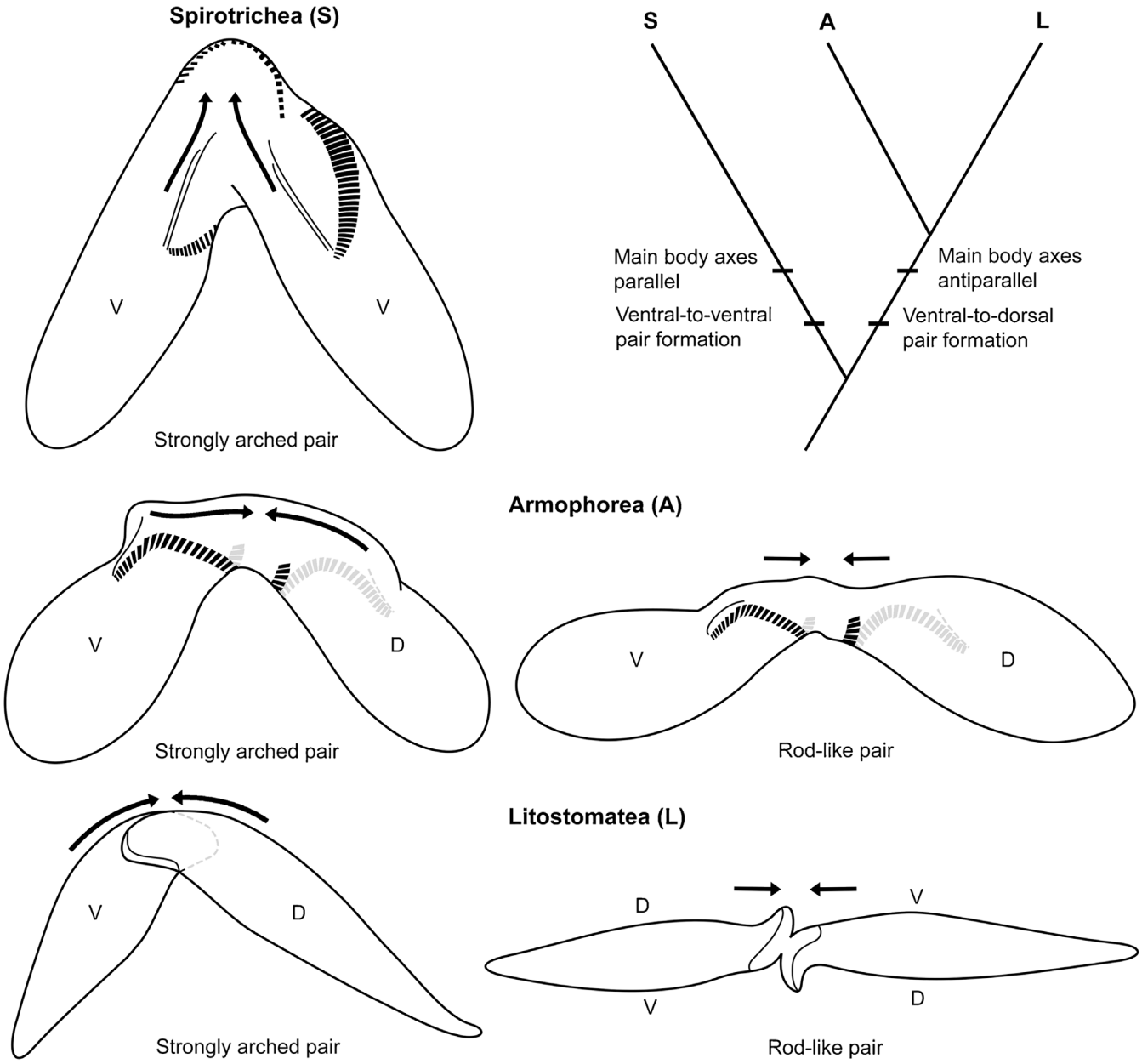

Fig. 11. Conjugation mode in the three main lineages of the SAL supercluster and their phylogenetic relationships as inferred from the arrangements of the partners during conjugation. Spirotricheans typically form strongly arched pairs and partners unite ventral-to-ventral. On the other hand, armophoreans and litostomateans form strongly arched to almost rod-like pairs and the partners unite ventral-to-dorsal. Arrows denote course of main body axis. SAL, genetic supercluster; D, dorsal; V, ventral.

so-called SAL supercluster (Chen et al. 2018; Gentekaki et al. 2014, 2017; Lynn and Kolisko 2017; Lynn et al. 2018). Recently, Maurer-Alcalá et al. (2018) suggested their genomic-architectural synapomorphy, viz., the presence of both nano-chromosomes and giant-chromosomes. Interestingly, giant-chromosomes were reported also from the classes Phyllopharyngea (Riley and Katz 2001) and Colpodea (Foissner 1993, p. 201) belonging to the so-called CONTHREEP supercluster. Extensive fragmentation of chromosomes into gene-sized nano-chromosomes during the development of macronucleus was, however, well documented only in the SAL supercluster and Phyllopharyngea but not in the Colpodea (for a review, see Maurer-Alcalá et al. 2018). These observations thus indicate that the presence of both nano-chromosomes and giant-chromosomes might have convergently evolved in the SAL supercluster and in the class Phyllopharyngea.

18S and 28S rRNA gene phylogenies have recently indicated that the bizarre and understudied Odontostomatea Fernandes et al., 2018 might also belong to the SAL supercluster (Fernandes et al. 2018). However, relationships among spirotricheans, armophoreans, litostomateans

and odontostomateans remain unresolved in these molecular analyses. Ultrastructural data and ontogenetic as well as conjugation peculiarities may help to cast some light on this problem. As we have already thoroughly discussed elsewhere, the cortex ultrastructure and ontogenesis indicate a sister group relationship of armophoreans and litostomateans (Foissner and Agatha 1999; Vďačný and Foissner 2017b; Vďačný et al. 2010). Detailed conjugation data have been not available for the armophoreans but helped to recognize the phylogenetic home of *Halteria grandinella*, a problematic spirotrichean taxon that morphologically appears like an oligotrich but clusters within the hypotrichs in 18S rRNA gene phylogenies (Foissner et al. 2004). The transient dimorphism of the partners and the common usage of the right conjugant's distal portion of the adoral zone during conjugation are shared features clearly uniting *Halteria* with other hypotrichs (Agatha and Foissner 2009). Likewise, a set of 124 genes supported the hypotrich home of *Halteria* and indicated its "oligotrich" features as a result of convergent evolution (Lynn and Kolisko 2017). On the other hand, *M. boletus* does not display any typical feature of the spirotrich conjugation mode, i.e., the partners do not unite ventral-to-ventral and their adoral zone is not modified during conjugation.

Interestingly, *M. boletus* shares some peculiar features with litostomateans during conjugation. Their conjugation mode is oblique to ventral-to-dorsal and the partners form strongly arched to almost rod-like pairs. In the rod-like arrangement, the main body axes are clearly antiparallel, which indicates that the true orientation of the partners is, indeed, heteropolar (Fig. 11). To date, heteropolar conjugation has been reliably reported only in litostomatean ciliates, for instance, in *Acaryophrya collaris*, *Didinium nasutum*, dileptids and spathidiids as well as in the endosymbiotic entodiniomorphids (Golińska and Afon'kin 1993; Prandtl 1906; Raikov 1972; Serrano et al. 1990; Vinnikova 1974; Vďačný and Foissner 2008, 2012; Visscher 1927; Xu and Foissner 2004). On the other hand, the main body axes are oriented in the same direction (homopolar) during conjugation in spirotricheans, such as euplotids, hypotrichs including halteriids, oligotrichs and choreotrichs (for a review, see Agatha and Foissner 2009). Moreover, pair formation is ventral-to-ventral in the vast majority of spirotricheans: the left anterior portion of one partner fuses with the right one of the other, so that their ventral sides face the substrate in hypotrichs (for reviews, see Berger 1999, 2006 and references cited therein); the ventral side of the partners overlap laterally or the ventral sides face in *Euplotes* (Diller 1966; Kloetzel 1975; Luporini and Dallai 1980); the ventral sides face in choreotrichs, oligotrichs and halteriids (Agatha and Foissner 2009 and references cited therein). The single exception seems to be the euplotid genus *Aspidisca* where the ventral side of the right conjugant covers the other partner dorsolaterally (Diller 1975; Rosati et al. 1998). However, the ventral-to-dorsal pairing occurs due to rotation after a brief ventral-to-ventral pair formation (Rosati et al. 1998), indicating that this is the plesiomorphic condition. Fusion of ventral sides is, indeed, widespread in ciliates and has been reported also from karyorelicteans (*Loxodes striatus* and *Tracheloraphis phoenicopterus*) and oligohymenophoreans (*Cryptochilum echini* and *Paramecium* spp.) (for review, see Raikov 1972).

Considering the phylogenetic relationships among the main spirotrichean lineages (e.g., Chen et al. 2018; Gentekaki et al. 2014, 2017; Lynn and Kolisko 2017; Lynn et al. 2018), the most parsimonious solution is that their last common ancestor (LCA) had a ventral-to-ventral and homopolar conjugation mode. On the other hand, the oblique to ventral-to-dorsal pair formation and the strongly arched to almost rod-like arrangement of the partners might be synapomorphies corroborating a sister group relationship of armophoreans and litostomateans (Fig. 11). This is further corroborated by (i) the plate-like arranged postciliary microtubule ribbons, forming a layer right of and between the ciliary rows; (ii) the purely somatic and telokinetal stomatogenesis beginning in the dorsal and dorsolateral kineties; (iii) the origin of the oral structures from migrating kinetofragments (Foissner and Agatha 1999; Vďačný and Foissner 2017b; Vďačný et al. 2010). Since phylogenetic relationships within the three classes of the SAL supercluster are not unambiguously resolved, one could argue that these features might be plesiomorphies of the last common ancestor of the SAL supercluster. However, it seems unlikely that so many specific ultrastructural, ontogenetic and conjugation features would be maintained in the LCAs of the classes Armophorea and Litostomatea but would be lost in the LCA of the class Spirotrichea. Therefore, we argue for their apomorphic nature supporting our Lamellicorticata hypothesis that Armophorea are the sister group of the Litostomatea (Vďačný et al. 2010).

Authors contributions

W.F. collected the sample and made the in vivo observations, micrographs, and all preparations. P.V. analyzed the protargol-impregnated slides, performed measurements and morphometric analyses, and made all drawings. Further, P.V. wrote most of the manuscript.

Acknowledgements

We are grateful to Dr. Barbara Harl and Robert Schörghofer for technical assistance. Financial support was provided by the Austrian Science Fund (FWF Project P26325_B16) and the Wilhelm and Ilse Foissner Stiftung. This work was supported also by the Slovak Research and Development Agency under the contract No. APVV-15-0147 and by the Grant Scientific Grant Agency of the Ministry of Education, Science, Research and Sport of the Slovak Republic and Slovak Academy of Sciences under the Grants VEGA 1/0041/17 and VEGA 1/0114/16.

References

Agatha, S., Foissner, W., 2009. Conjugation in the spirotrich ciliate *Halteria grandinella* (Müller, 1773) Dujardin, 1841 (Protozoa, Ciliophora) and its phylogenetic implications. Eur. J. Protistol. 45, 51–63.

Berger, H., 1999. Monograph of the Oxytrichidae (Ciliophora, Hypotrichia). Monogr. Biol. 78, 1–1080.

Berger, H., 2006. Monograph of the Urostyloidea (Ciliophora, Hypotricha). Monogr. Biol. 85, 1–1304.

Bourland, W.A., Wendell, L., 2014. Redescription of *Atopospira galeata* (Kahl, 1927) nov. comb. and *A. violacea* (Kahl, 1926) nov. comb. with redefinition of *Atopospira* Jankowski, 1964 nov. stat. and *Brachonella* Jankowski, 1964 (Ciliophora, Armophorida). Eur. J. Protistol. 50, 356–372.

Bourland, W.A., Wendell, L., Hampikian, G., 2014. Morphologic and molecular description of *Metopus fuscus* Kahl from North America and new rDNA sequences from several metopids (Armophorea, Metopidae). Eur. J. Protistol. 50, 213–230.

Bourland, W., Rotterová, J., Čepička, I., 2017. Redescription and molecular phylogeny of the type species for two main metopid genera, *Metopus es* (Müller, 1776) Lauterborn, 1916 and *Brachonella contorta* (Levander, 1894) Jankowski, 1964 (Metopida, Ciliophora), based on broad geographic sampling. Eur. J. Protistol. 59, 133–154.

Bourland, W., Rotterová, J., Luo, X., Čepička, I., 2018. The little-known freshwater metopid ciliate, *Idiometopus turbo* (Dragesco and Dragesco-Kernéis, 1986) nov. gen., nov. comb., originally discovered in Africa, found on the Micronesian island of Guam. Protist 169, 494–506.

Bütschli, O., 1889. Protozoa. Abt. III. Infusoria und system der radiolaria. In: Bronn, H.G. (Ed.), Klassen und Ordnung des Thier-Reichs, Vol. I. C. F. Winter, Leipzig, pp. 1098–2035.

Chen, X., Wang, Y., Sheng, Y., Warren, A., Gao, S., 2018. GPSit: an automated method for evolutionary analysis of nonculturable ciliated microeukaryotes. Mol. Ecol. Resour. 18, 700–713.

Corliss, J.O., 1979. The Ciliated Protozoa. Characterization, Classification, and Guide to the Literature, 2nd ed. Pergamon Press, Oxford.

da Silva-Neto, I.D., da Silva Paiva, T., do Nascimento Borges, B., Harada, M.L., 2016. Fine structure and molecular phylogeny of *Parametopidium circumlabens* (Ciliophora: Armophorea), endocommensal of sea urchins. J. Eukaryot. Microbiol. 63, 46–51.

de Puytorac, P., Grain, J., 1976. Ultrastructure du cortex buccal et évolution chez les ciliés. Protistologica 12, 49–67.

Diller, W.F., 1966. Correlation of ciliary and nuclear development in the life cycle of *Euplotes*. J. Protozool. 13, 43–54.

Diller, W.F., 1975. Nuclear behavior and morphogenetic changes in fission and conjugation of *Aspidisca costata* (Dujardin). J. Protozool. 22, 221–229.

Doflein, F., Reichenow, E., 1929. Lehrbuch der Protozoenkunde. Eine Darstellung der Naturgeschichte der Protozoen mit besonderer Berücksichtigung der parasitischen und pathogenen Formen, 5th ed. G. Fischer, Jena.

Dragesco, J., Dragesco-Kernéis, A., 1986. Ciliés libres de l'Afrique intertropicale. Introduction à la connaissance et à l'étude des ciliés. Faune tropicale (Éditions de l'Orstom, Paris) 26, 1–559.

Embley, T.M., Finlay, B.J., 1994. The use of small subunit rRNA sequences to unravel the relationships between anaerobic ciliates and their methanogen endosymbionts. Microbiology 140, 225–235.

Fernandes, N.M., Vizzoni, V.F., Borges, B.D.N., Soares, C.A.G., da Silva-Neto, I.D., Paiva, T.D.S., 2018. Molecular phylogeny and comparative morphology indicate that odontostomatids (Alveolata, Ciliophora) form a distinct class-level taxon related to Armophorea. Mol. Phylogenet. Evol. 126, 382–389.

Foissner, W., 1993. Colpodea (Ciliophora). Protozoenfauna 4, 1–798.

Foissner, W., 2014. An update of 'basic light and scanning electron microscopic methods for taxonomic studies of ciliated protozoa'. Int. J. Syst. Evol. Microbiol. 64, 271–292.

Foissner, W., 2016a. Terrestrial and semiterrestrial ciliates (Protozoa, Ciliophora) from Venezuela and Galápagos. Denisia 35, 1–912.

Foissner, W., 2016b. *Heterometopus meisterfeldi* nov. gen., nov. spec. (Protozoa, Ciliophora), a new metopid from Australia. Eur. J. Protistol. 55, 118–127.

Foissner, W., Agatha, S., 1999. Morphology and morphogenesis of *Metopus hasei* Sondheim, 1929 and *M. inversus* (Jankowski, 1964) nov. comb. (Ciliophora, Metopida). J. Eukaryot. Microbiol. 46, 174–193.

Foissner, W., Berger, H., Kohmann, F., 1992. Taxonomische und ökologische Revision der Ciliaten des Saprobiensystems – Band II: Peritrichia, Heterotrichida, Odontostomatida. Informationsberichte des Bayer. Landesamtes für Wasserwirtschaft 5 (92), 1–502.

Foissner, W., Agatha, S., Berger, H., 2002. Soil ciliates (Protozoa, Ciliophora) from Namibia (Southwest Africa), with emphasis on two contrasting environments, the Etosha region and the Namib Desert. Denisia 5, 1–1459.

Foissner, W., Moon-van der Staay, S.Y., van der Staay, G.W.M., Hackstein, J.H.P., Krautgartner, W.-D., Berger, H., 2004. Reconciling classical and molecular phylogenies in the stichotrichines (Ciliophora, Spirotrichea), including new sequences from some rare species. Eur. J. Protistol. 40, 265–281.

Gentekaki, E., Kolisko, M., Boscaro, V., Bright, K.J., Dini, F., Di Giuseppe, G., Gong, Y., Miceli, C., Modeo, L., Molestina, R.E., Petroni, G., Pucciarelli, S., Roger, A.J., Strom, S.L., Lynn, D.H., 2014. Large-scale phylogenomic analysis reveals the phylogenetic position of the problematic taxon *Protocruzia* and unravels the deep phylogenetic affinities of the ciliate lineages. Mol. Phylogenet. Evol. 78, 36–42.

Gentekaki, E., Kolisko, M., Gong, Y., Lynn, D., 2017. Phylogenomics solves a long-standing evolutionary puzzle in the ciliate world: the subclass Peritrichia is monophyletic. Mol. Phylogenet. Evol. 106, 1–5.

Golikowa, M.N., 1965. Der Aufbau des Kernapparates und die Verteilung der Nukleinsäuren und Proteine bei *Nyctotherus cordiformis* Stein. Arch. Protistenk. 108, 191–216.

Golińska, K., Afon'kin, S.Yu., 1993. Preparatory changes and the development of the conjugation junction in a ciliate, *Dileptus*. Protoplasma 173, 144–157.

Hammerschmidt, B., Schlegel, M., Lynn, D.H., Leipe, D.D., Sogin, M.L., Raikov, I.B., 1996. Insights into the evolution of nuclear dualism in the ciliates revealed by phylogenetic analysis of rRNA sequences. J. Eukaryot. Microbiol. 43, 225–230.

Hirt, R.P., Dyal, P.L., Wilkinson, M., Finlay, B.J., Roberts, D.-Mc L., Embley, T.M., 1995. Phylogenetic relationship among karyorelictids and heterotrichs inferred from small subunit rRNA

sequences: resolution at the base of the ciliate tree. Mol. Phylogenet. Evol. 4, 77–87.
International Commission on Zoological Nomenclature (ICZN), 1999. International Code of Zoological Nomenclature, 4th ed. Tipografia La Garangola, Padova.
International Commission on Zoological Nomenclature (ICZN), 2012. Amendment of Articles 8, 9, 10, 21 and 78 of the International Code of Zoological Nomenclature to expand and refine methods of publication. Bull. Zool. Nomencl. 69, 161–169.
Jankowski, A.W., 1964. Morphology and evolution of Ciliophora. III. Diagnoses and phylogenesis of 53 sapropelebionts, mainly of the order Heterotrichida. Arch. Protistenk. 107, 185–294.
Jankowski, A.W., 1980. Konspekt novoj sistemy tipa Ciliophora (Conspectus of a new system of the phylum Ciliophora). Trudy Zool. Inst., Leningrad 94, 103–121 (in Russian).
Kahl, A., 1926. Neue und wenig bekannte Formen der holotrichen und heterotrichen Ciliaten. Arch. Protistenk. 55, 198–438.
Kahl, A., 1927. Neue und ergänzende Beobachtungen heterotricher Ciliaten. I. Arch. Protistenk. 57, 121–203.
Kahl, A., 1929. Persönliche Erwiderung auf Wetzel's Kritik an meiner Bearbeitung der Gattung *Metopus* (Infusoria heterotricha). Z. Morphol. Ökol. Tiere 15, 723–734.
Kahl, A., 1932. Urtiere oder Protozoa I: Wimpertiere oder Ciliata (Infusoria) 3. Spirotricha. Tierwelt Dtl. 25, 399–650.
Kloetzel, J.A., 1975. Scanning electron microscopy of stomatogenesis accompanying conjugation in *Euplotes aediculatus*. J. Protozool. 22, 385–392.
Lauterborn, R., 1916. Die sapropelische Lebewelt. Ein Beitrag zur Biologie des Faulschlammes natürlicher Gewässer. Verh. Naturkundl. Med. Ver. Heidelb. 13, 395–481.
Luporini, P., Dallai, R., 1980. Sexual interaction of *Euplotes crassus*: differentiation of cellular surfaces in cell-to-cell union. Dev. Biol. 77, 167–177.
Lynn, D.H., 2004. Morphology or molecules: how do we identify the major lineages of ciliates (Phylum Ciliophora)? Eur. J. Protistol. 39, 356–364.
Lynn, D.H., Kolisko, M., 2017. Molecules illuminate morphology: phylogenomics confirms convergent evolution among 'oligotrichous' ciliates. Int. J. Syst. Evol. Microbiol. 67, 3676–3682.
Lynn, D.H., Small, E.B., 2002. Phylum Ciliophora. In: Lee, J.J., Leedale, G.F., Bradbury, P. (Eds.), An Illustrated Guide to the Protozoa, Organisms traditionally Referred to as Protozoa, or Newly Discovered Groups. , 2nd ed. Society of Protozoologists, Lawrence, Kansas, pp. 371–656.
Lynn, D.H., Kolisko, M., Bourland, W., 2018. Phylogenomic analysis of *Nassula variabilis* n. sp., *Furgasonia blochmanni*, and *Pseudomicrothorax dubius* confirms a nassophorean clade. Protist 169, 180–189.
Maurer-Alcalá, X.X., Yan, Y., Pilling, O.A., Knight, R., Katz, L.A., 2018. Twisted tales: insights into genome diversity of ciliates using single-cell 'omics. Genome Biol. Evol. 10, 1927–1939.
Müller, O.F., 1776. Zoologiae Danicae Prodromus, seu Animalium Daniae et Norvegiae Indigenarum Characteres, Nomina, et Synonyma Imprimis Popularium. Typis Hallageriis, Havniae.
Noland, L.E., 1927. Conjugation in the ciliate *Metopus sigmoides* C. and L. J. Morphol. 44, 341–361.
Omar, A., Zhang, Q., Zou, S., Gong, J., 2017. Morphology and phylogeny of the soil ciliate *Metopus yantaiensis* n. sp. (Ciliophora, Metopida), with identification of the intracellular bacteria. J. Eukaryot. Microbiol. 64, 792–805.
Prandtl, H., 1906. Die Konjugation von *Didinium nasutum* O. F. M. Arch. Protistenk. 7, 229–258.
Raikov, I.B., 1972. Nuclear phenomena during conjugation and autogamy in ciliates. In: Chen, T.-T. (Ed.), Research in Protozoology. Pergamon Press, Oxford, pp. 146–289.
Riley, J.L., Katz, L.A., 2001. Widespread distribution of extensive chromosomal fragmentation in ciliates. Mol. Biol. Evol. 18, 1372–1377.
Rosati, G., Verni, F., Dini, F., 1998. Mating by conjugation in two species of the genus *Aspidisca* (Ciliata, Hypotrichida): an electron microscopic study. Zoomorphology 118, 1–12.
Serrano, S., Martín-González, A., Fernández-Galiano, D., 1990. General morphology and cytological events during the conjugation process in *Acaryophrya collaris* (Kahl, 1926) (Ciliophora, Haptorina). Arch. Protistenk. 138, 65–74.
Small, E.B., Lynn, D.H., 1981. A new macrosystem for the phylum Ciliophora Doflein, 1901. BioSystems 14, 387–401.
Tirjaková, E., Krajčovičová, K., Illyová, M., Vďačný, P., 2016. Interaction of ciliate communities with cyanobacterial water bloom in a shallow, hypertrophic reservoir. Acta Protozool. 55, 173–188.
Vďačný, P., Foissner, W., 2008. Morphology, conjugation, and postconjugational reorganization of *Dileptus tirjakovae* n. sp. (Ciliophora, Haptoria). J. Eukaryot. Microbiol. 55, 436–447.
Vďačný, P., Foissner, W., 2012. Monograph of the dileptids (Protista, Ciliophora, Rhynchostomatia). Denisia 31, 1–529.
Vďačný, P., Foissner, W., 2017a. A huge diversity of metopids (Ciliophora, Armophorea) in soil from the Murray River floodplain, Australia. I. Description of five new species and redescription of *Metopus setosus* Kahl, 1927. Eur. J. Protistol. 57, 35–76.
Vďačný, P., Foissner, W., 2017b. A huge diversity of metopids (Ciliophora, Armophorea) in soil from the Murray River floodplain, Australia. II. Morphology and morphogenesis of *Lepidometopus platycephalus* nov. gen., nov. spec. Acta Protozool. 56, 39–57.
Vďačný, P., Orsi, W., Foissner, W., 2010. Molecular and morphological evidence for a sister group relationship of the classes Armophorea and Litostomatea (Ciliophora, Intramacronucleata, Lamellicorticata infraphyl. nov.), with an account on basal haptorid litostomateans. Eur. J. Protistol. 46, 298–309.
Vďačný, P., Rajter, Ľ., Stoeck, T., Foissner, W., 2019. A proposed timescale for the evolution of armophorean ciliates: clevelandellids diversify more rapidly than metopids. J. Eukaryot. Microbiol. 66, 167–181.
Vinnikova, N.V., 1974. Conjugation in *Dileptus anser* (O. F. M.) (Gymnostomatida, Tracheliidae). Acta Protozool. 12, 275–287 (in Russian with English summary).
Visscher, J.P., 1927. Conjugation in the ciliated protozoon, *Dileptus gigas*, with special reference to the nuclear phenomena. J. Morphol. 44, 383–415.
Wichterman, R., 1937. Division and conjugation in *Nyctotherus cordiformis* (Ehr.) Stein (Protozoa, Ciliata) with special reference to the nuclear phenomena. J. Morphol. 60, 563–611.
Xu, K., Foissner, W., 2004. Body, nuclear, and ciliary changes during conjugation of *Protospathidium serpens* (Ciliophora, Haptoria). J. Eukaryot. Microbiol. 51, 605–617.